iScience

CellPress
OPEN ACCESS

Article

LAPTM4B-YAP loop feedback amplification enhances the stemness of hepatocellular carcinoma

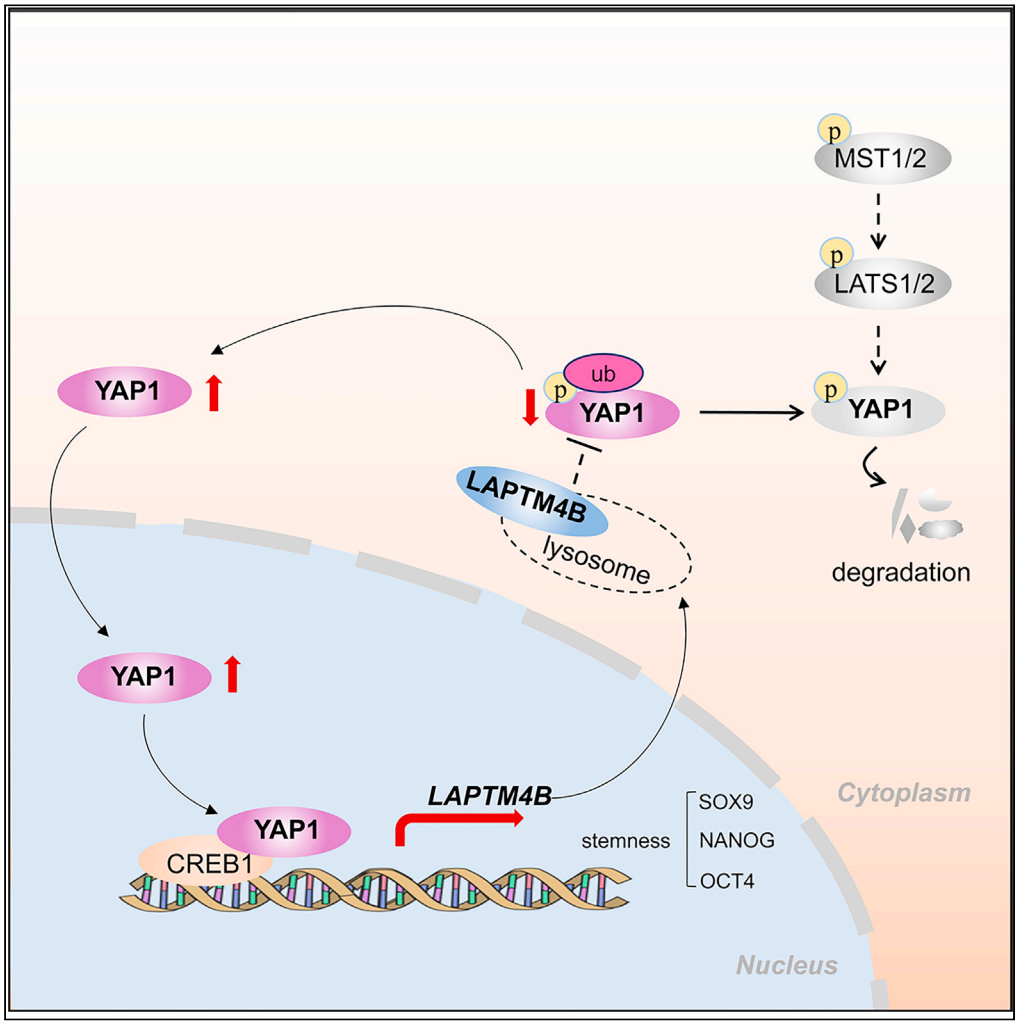

Jianping Liao, Jiahong Wang, Yu Xu, ..., Yan Meng, Lixin Wei, Aimin Huang

karenmeng0521@163.com (Y.M.)
weilixin_smmu@163.com (L.W.)
aimin@fjmu.edu.cn (A.H.)

Highlights

LAPTM4B is essential for the stemness maintenance of HCC tumor cells

LAPTM4B inhibits YAP phosphorylation and ubiquitination degradation

YAP promotes the transcription of LAPTM4B by binding to CREB1

Hyperactivation of the LAPTM4B-YAP loop predicts a poor prognosis in HCC patients

Liao et al., iScience 26, 106754
June 16, 2023
https://doi.org/10.1016/j.isci.2023.106754

iScience

CellPress
OPEN ACCESS

Article

LAPTM4B-YAP loop feedback amplification enhances the stemness of hepatocellular carcinoma

Jianping Liao,[1,4,5] Jiahong Wang,[1,5] Yu Xu,[1,5] Yong Wu,[1] Meifeng Wang,[1] Qiudong Zhao,[2] Xiaodan Tan,[1] Yan Meng,[2,3,*] Lixin Wei,[2,*] and Aimin Huang[1,6,*]

SUMMARY

Hepatocellular carcinoma (HCC) is highly heterogeneous, and stemness signatures are frequently elevated in HCC tumor cells to generate heterogeneous subtypes via multidirectional differentiation. However, the mechanisms affecting the regulation of stemness in HCC remain unclear. In this study, we identified that lysosome-associated protein transmembrane-4β (LAPTM4B) was significantly overexpressed in stem-like tumor cell populations with multidirectional differentiation potential at the single cell level, and verified that LAPTM4B was closely related to stemness of HCC using *in vitro* and *in vivo* experiments. Mechanistically, elevated LAPTM4B suppresses Yes-associated protein (YAP) phosphorylation and ubiquitination degradation. In turn, stabilized YAP localizes to the nucleus and binds to cAMP responsive element binding protein-1 (CREB1), which promotes transcription of LAPTM4B. Overall, our findings suggest that LAPTM4B forms a positive feedback loop with YAP, which maintains the stemness of HCC tumor cells and leads to an unfavorable prognosis for HCC patients.

INTRODUCTION

Hepatocellular carcinoma (HCC) is one of the most lethal tumor types globally, with approximately half of new cases and deaths worldwide occurring in China.[1,2] HCC presents a highly heterogeneous malignancy, leading to extremely limited and significant individual differences in treatment improvement. Current studies suggest that the formation of heterogeneity in HCC and its resulting poor prognosis are partially driven by the stemness of tumor cells.[3,4] The stem properties of tumor cells are manifested in their capacities for self-renewal and generation of heterogeneous progenies,[5] which endows HCC with a high capacity to adapt to the external environment or resist treatment, predicting the progression of HCC.[6,7] However, the molecular mechanisms of the stemness maintenance of HCC tumor cells remain unclear.

Lysosome-associated protein transmembrane-4β (*LAPTM4B*), a member of the LAPTM family, was first identified in HCC by fluorescence differential display.[8] LAPTM4B, a four-transmembrane protein that is closely associated with the lysosomal function,[9] regulates biological processes, including signaling across membranes, membrane sorting and protein degradation,[10,11] particularly ubiquitin-dependent degradation. Impressively, the level of LAPTM4B is barely detectable in normal liver tissues, but it is dramatically increased in HCC.[12] It functions as an oncogene that participates in promoting the growth, progression and multidrug resistance of HCC.[13,14] There is strong evidence for the role of LAPTM4B in hepatocarcinogenesis, and its expression level is positively correlated with the progression and malignancy of HCC.[15,16] In addition, LAPTM4B has been reported to be proposed as an independent prognostic factor of HCC patients. However, whether and how LAPTM4B affects stemness in HCC remains poorly understood.

The Hippo signaling pathway is a conserved signaling module composed of a kinase cascade that is known to regulate stem cell homeostasis and tumorigenesis.[17] The transcriptional coactivator Yes-associated protein (YAP) is the central player in that pathway and is negatively regulated by the upstream cascade kinase, including MST1/2 and LATS1/2.[18] Following the inactivation of canonical Hippo signaling, stabilized YAP can enter the nucleus and subsequently transfer biological signals, thus promoting the transcription of downstream target genes.[19] The active state transition of YAP is involved in stem cell proliferation, differentiation and tumorigenesis.[18] Upregulation of YAP protein levels and nuclear accumulation has been observed in several tumor tissues including HCC.[20] Hyperactivation of YAP has been proven to directly or indirectly control the proliferation, invasion and metastasis of HCC.[21] Furthermore, YAP overactivation

[1]Department of Pathology, School of Basic Medical Sciences, Fujian Medical University, 88 Jiaotong Road, Fuzhou, Fujian 350004, China

[2]Tumor Immunology and Gene Therapy Center, Third Affiliated Hospital of Second Military Medical University, 225 Changhai Road, Shanghai 200438, China

[3]Department of Medical Ultrasound, Shanghai Tenth People's Hospital, Tongji University Cancer Center, Tongji University School of Medicine, Shanghai 200072, China

[4]Sun Yat-sen University Cancer Center, State Key Laboratory of Oncology in South China, Guangzhou 510060, China

[5]These authors contributed equally

[6]Lead contact

*Correspondence: karenmeng0521@163.com (Y.M.), weilixin_smmu@163.com (L.W.), aimin@fjmu.edu.cn (A.H.)

https://doi.org/10.1016/j.isci.2023.106754

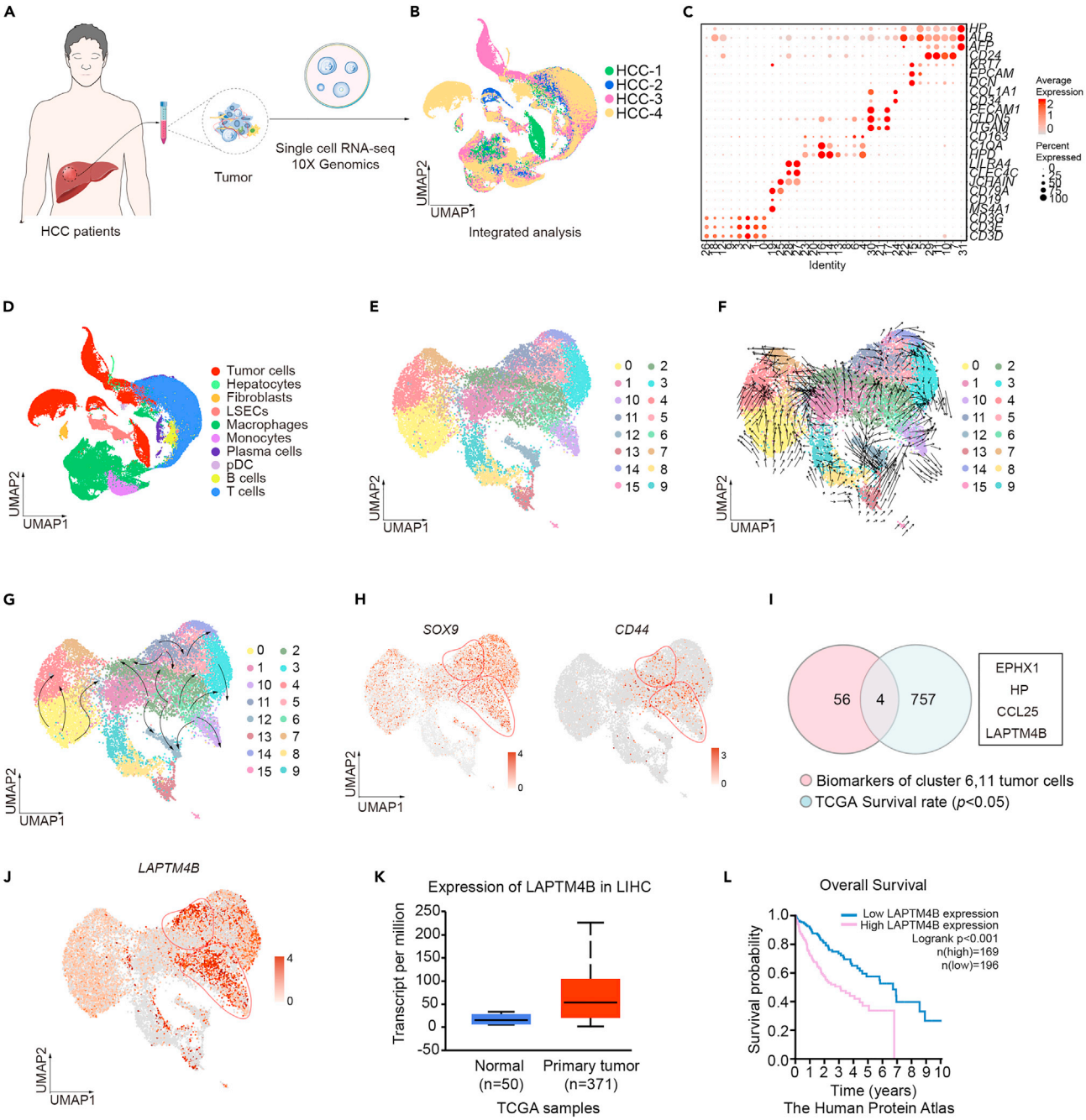

Figure 1. Elevated LAPTM4B was observed in stem-like tumor cells in HCC patients

(A) Schematic of the experimental workflow of liver tumor tissue collection, processing, sequencing and data analysis.

(B) Uniform manifold approximation and projection (UMAP) plot of all single cells from 4 HCC patients (indicated by colors). The case IDs were named HCC-1 to 4.

(C) Dot plots showing the expression of known lineage-specific marker genes in each cell cluster (circle size indicating the percent expressed and color representing average expression).

(D) UMAP plot of all cell types (indicated by colors).

(E) UMAP plot showing 16 clusters of all single tumor cells.

(F) RNA velocity field superimposed on the UMAP embedding of tumor cells.

(G) The UMAP uniform manifold approximation and projection in 1F.

(H) UMAP expression maps of *SOX9* and *CD44* in tumor cells. The color bar indicates log2 normalized expression.

(I) The integrative analysis combined scRNA-seq data and the publicly available database in liver cancer from The Cancer Genome Atlas (TCGA) database.

Figure 1. *Continued*
(J) UMAP expression maps of *LAPTM4B* in tumor cells. The color bar indicates log2 normalized expression.
(K) The expression of LAPTM4B in normal (n = 50) and tumor (n = 371) tissues of HCC patients from the TCGA database.
(L) Kaplan-Meier survival analysis of patients with LAPTM4B at high or low levels from the human protein atlas.
See also Figures S1 and S2.

confers cancer stem cell-like features in HCC tumor cells, contributing to the poor response to the treatment of HCC patients.[22] Also, in most models, YAP-driven hepatic overgrowth is observed mainly by the activation and expansion of progenitor cells. In mouse and human hepatocarcinogenesis, YAP can regulate hepatocyte plasticity and tumor heterogeneity by upregulating SOX9 activity.[23] Our previous study has shown that collagen-stimulated YAP-signaling hyperactivation contributes to transcriptional diversity through upregulating stemness in liver cancer.[24] However, the regulatory mechanism of YAP in stemness maintenance in HCC is not well defined.

In this study, we observed the overexpression of LAPTM4B in tumor cells possessing the potential to differentiate into heterogeneous subpopulations in HCC patients at the single-cell level. Furthermore, we demonstrated the important role of LAPTM4B in the stemness maintenance of HCC tumor cells. Mechanistically, LAPTM4B might act as an inhibitor of the ubiquitin-dependent degradation of YAP to regulate the stemness of HCC tumor cells. In response, YAP bound to cAMP responsive element binding protein-1 (CREB1) and promoted the transcription of LAPTM4B. The above-mentioned integration of LAPTM4B and YAP in driving activation of each other constituted a positive feedback system, driving enhanced stemness of tumor cells and suggesting a poor prognosis for HCC patients. Thus, our study provided potential mechanistic insights into the regulation of stemness during HCC progression, regarding clinical implications for the treatment of HCC.

RESULTS

scRNA-seq identifies overexpressed LAPTM4B in stem-like tumor cells in HCC patients

To investigate the molecular and cellular characteristics of hepatocellular carcinoma (HCC), we conducted single-cell RNA sequencing (scRNA-seq) using specimens from 4 clinical patients (Figure 1A). The uniform manifold approximation and projection (UMAP) dimensionality reduction was utilized to visualize[25] the information of all samples and 31 clusters were identified in the combined dataset (Figures 1B and S1A). In total, 90 945 single-cell transcriptomes were captured after initial quality controls. Further clustering analyses yielded 10 major cell type identities mainly based on their marker genes, including hepatocytes, fibroblasts, liver sinusoidal endothelial cells (LSECs), macrophages, monocytes, plasma cells (PCs), dendritic cells (DCs), B cells, T cells and tumor cells (Figures 1C, 1D, and S1B).

We next extracted tumor cells and studied their characteristic (Figures S1C and 1E). Notably, RNA velocity analysis exhibited a manifold with multiple branches from the center (especially clusters 6,11) to peripheral tumor cells (clusters 2, 3, 5, 10 and 12) (Figures 1F and 1G), suggesting clusters 6 and 11 potentially possessed the signatures of multidirectional differentiation to generate heterogeneous tumor cells. Consistent with this result, the stemness molecules *SOX9*[26] and *CD44*[27] were significantly elevated in these subsets (clusters 6,11), which might be stem-like tumor cells (Figure 1H). Subsequent integrative analysis of the specific biomarkers of this stem-like tumor cell subsets and survival-related genes in HCC from the Cancer Genome Atlas (TCGA) database enabled us to focus on 4 promising candidates (*EPHX1*, *HP*, *CCL25* and *LAPTM4B*) (Figure 1I). Moreover, we further analyzed the expression profiles of *EPHX1*, *HP*, *CCL25* and *LAPTM4B* (Figures S1D and 1J). A co-occurrence pattern of *SOX9, CD44* and *LAPTM4B* in stem-like tumor cell subsets was observed (Figures 1H and 1J). The trajectory of malignant cells in every patient based on the reversed graph embedding method. Of interest, we found branches with accumulation of LAPTM4B tend to be aggregated at the trunk of the trajectory tree, suggesting that LAPTM4B was highly expressed in the initial segment, i.e., stem cell-like cells with differentiation potential (Figure S2A). Furthermore, correlation analysis showed moderately high correlation of *SOX9*, *CD44* and *LAPTM4B* (Figure S2B). Indeed, the gene set variation analysis (GSVA) data exhibited that enrichments of stem genes among tumor samples were closely related to the expression of LAPTM4B (Figure S2C), indicating a potential regulation of *LAPTM4B* in stem-like HCC tumor cells. To further confirm the co-expression profiles of SOX9, CD44 and LAPTM4B, we examined the expression of SOX9, CD44 and LAPTM4B in HCC datasets available from the TCGA and tissue microarrays containing 105 HCC specimens. Positive correlations between *SOX9*, *CD44* and *LAPTM4B* were observed in TCGA datasets (Figure S2D). Moreover, elevated expression of LAPTM4B

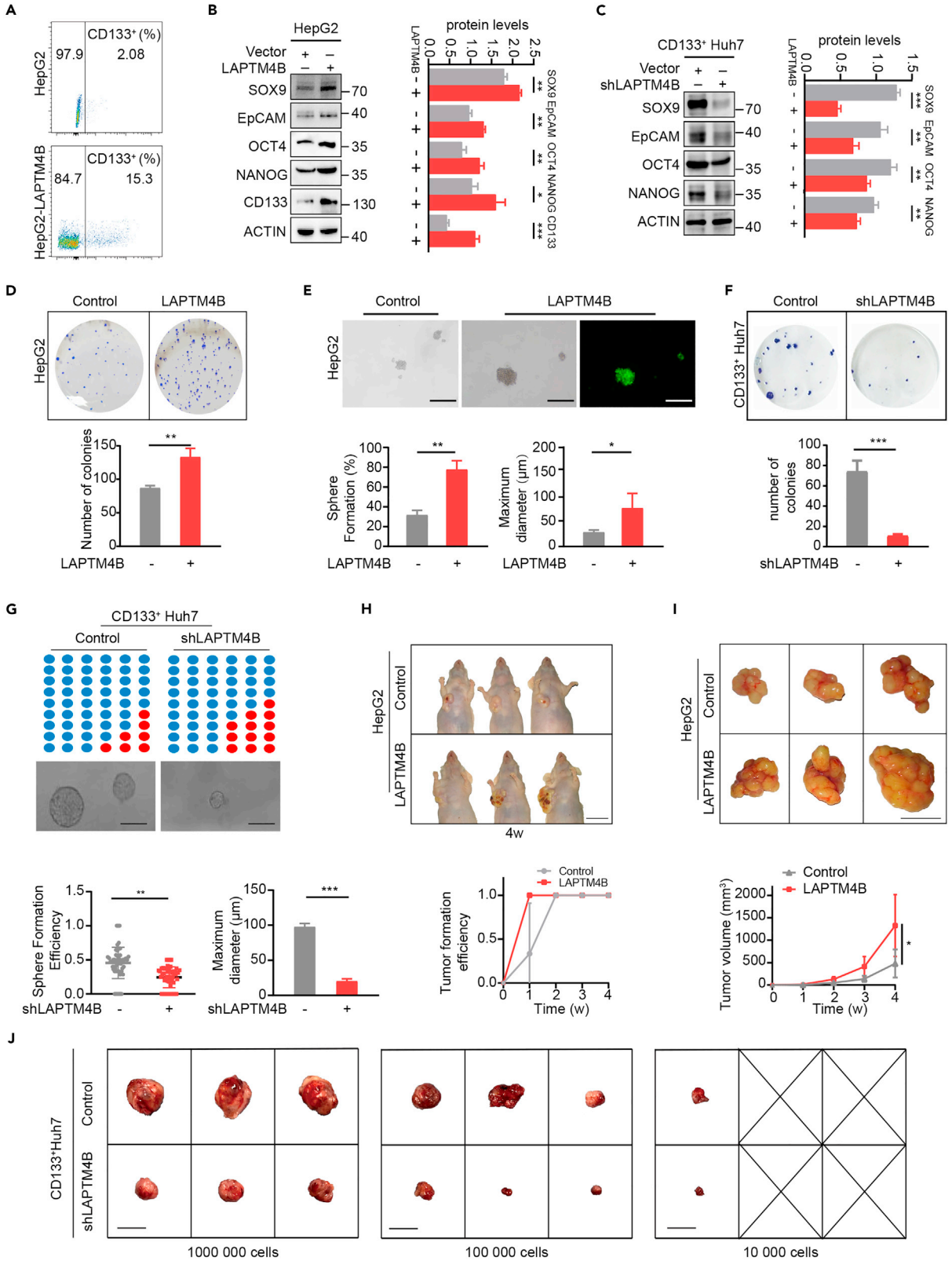
A
HepG2
97.9
CD133⁺ (%)
2.08
HepG2-LAPTM4B
84.7
CD133⁺ (%)
15.3
B
HepG2
Vector
LAPTM4B
SOX9
EpCAM
OCT4
NANOG
CD133
ACTIN
70
40
35
35
130
40
protein levels
SOX9
EpCAM
OCT4
NANOG
CD133
C
CD133⁺ Huh7
Vector
shLAPTM4B
protein levels
D
Control
LAPTM4B
HepG2
Number of colonies
LAPTM4B
E
Control
LAPTM4B
HepG2
Sphere Formation (%)
Maximum diameter (μm)
F
Control
shLAPTM4B
CD133⁺ Huh7
number of colonies
shLAPTM4B
G
CD133⁺ Huh7
Control
shLAPTM4B
Sphere Formation Efficiency
Maximum diameter (μm)
H
HepG2
Control
LAPTM4B
4w
Tumor formation efficiency
Time (w)
I
HepG2
Control
LAPTM4B
Tumor volume (mm³)
Time (w)
J
CD133⁺Huh7
Control
shLAPTM4B
1000 000 cells
100 000 cells
10 000 cells

Figure 2. LAPTM4B promotes stemness properties in HepG2 cells

(A) Flow cytometry observed the proportion of CD133-positive cells in HepG2 cells transfected with LAPTM4B or vector.

(B) Western blotting assays of CD133, EpCAM, NANOG, OCT4 and SOX9 levels in control cells and LAPTM4B overexpressed HepG2 cells.

(C) Western blotting assays of EpCAM, NANOG, OCT4 and SOX9 levels in $CD133^+$ Huh7 cells with or without LAPTM4B-knockdown.

(D) (Top) Representative photographs of stained colonies after the colony-formation assay. (Bottom) The number of colonies of HepG2 cells with or without LAPTM4B-overexpressing.

(E) The capacity of clones detected by sphere formation assays in HepG2 cells for 5 days. Bar, 100 μm.

(F) (Top) Representative photographs of stained colonies after the colony-formation assay. (Bottom) The number of colonies of $CD133^+$ Huh7 cells with or without LAPTM4B-knockdown.

(G) Self-renewal ability was detected by the sphere limiting dilution assay in $CD133^+$ Huh7 cells for 5 days. Bar, 100 μm.

(H and I) Subcutaneous xenograft assay detected the tumor formation ability of HepG2 cells with or without LAPTM4B-overexpressing (n = 3 per group).

(J) *In vivo* tumorigenicity assay with limited dilution (n = 3 per group). At least two independent experiments were performed for all data. For curve figures and bar figures, data are presented as means ± SD. Unpaired Student's *t* tests were used for comparing two variables. One-way ANOVA was used for multiple variables comparison. *, $p< 0.05$; **, $p< 0.01$; ***, $p< 0.001$; n.s., no significance in comparison with control group.

See also Figure S3.

and its co-expression with SOX9 were observed in HCC tissues (Figure S2E). Meanwhile, highly similar staining patterns were observed for CD44, strongly indicating co-expression profiles of LAPTM4B and SOX9 in patients with HCC (Figures S2E–S2H). In addition, we interrogated the TCGA database to evaluate LAPTM4B in HCC patients. The mRNA level of *LAPTM4B* was significantly elevated in HCC patient specimens (n = 371) compared to normal tissues (n = 50) (Figure 1K, HR (high) = 1.8, p = 0.0014). Similarly, in the human protein atlas, patients with tumors expressing LAPTM4B mRNA at the upper level (High LAPTM4B TPM) had a significantly shorter overall survival time than patients with tumors expressing LAPTM4B at the lower (Figure 1L). Altogether, these observations suggested that LAPTM4B was involved in the maintenance of stem characteristics in cancer stem-like cells in HCC.

LAPTM4B maintains stemness in HCC tumor cells

To elucidate the role of LAPTM4B in the enhancement of stemness in HCC tumor cells, we first sorted $CD133^+$ (stemness-related marker[28]) tumor cells from HepG2 or Huh7 HCC cell lines to simulate stem-like tumor cells. Then, we generated LAPTM4B overexpressed HepG2 cells and LAPTM4B silenced $CD133^+$ HepG2 cells by a lentiviral-mediated system. A more than 3-fold change of LAPTM4B was detected at mRNA and protein levels in lentivirus-treated cells compared with the control group (Figures S3A–S3F). Of interest, flow cytometry and western blotting revealed that overexpression of LAPTM4B increased the proportion of $CD133^+$ cells in HepG2 cells (Figures 2A and 2B). The expression profiles of three stemness-associated genes (*SOX9*, *OCT4*,[29] and *NANOG*[30]) and one stem cell surface marker (*EpCAM*[31]) were elevated when cells overexpression of LAPTM4B match the control group, especially at the protein level (Figures 2B and S3G). Silencing LAPTM4B in $CD133^+$ Huh7 cells observed opposite results (Figures 2C and S3H). Consistent with this result, LAPTM4B overexpressing resulted in an increasing colony-formation ability (Figure 2D) and sphere numbers and size compared with the control group in HepG2 cell lines (Figure 2E). On the contrary, knockdown of LAPTM4B decreased the abilities of clone and sphere formation in $CD133^+$ Huh7 cells (Figures 2F and 2G). Furthermore, we examined the tumor-initiating capacity by injecting 5×10^6 HepG2 cells with or without LAPTM4B-overexpressing subcutaneously into nude mice for 4 weeks. Mice injected with LAPTM4B-overexpressing HepG2 cells significantly shortened the time of tumor formation (Figure 2H), and increased tumor size compared with the control group (Figure 2I), which indicated that LAPTM4B enhanced the tumor formation ability of HepG2 cells. The limiting dilution subcutaneous xenografts showed that LAPTM4B silenced $CD133^+$ Huh7 cells reduced the capacity to form tumors in mice (Figure 2J). Similar results were observed in the Huh7 cell line (Figures S3H–S3J). Altogether, these observations suggested that LAPTM4B was required for the maintenance of stem characteristics in HCC tumor cells.

LAPTM4B enhances the transcriptional activation and nuclear localization of YAP

To explore the mechanisms by which LAPTM4B regulates stemness in HCC, we performed RNA-seq analysis to evaluate the global impact of LAPTM4B on HCC tumor cells. Compared with the control group, 712 genes were significantly downregulated in LAPTM4B knockdown $CD133^+$ Huh7 cells, including some stemness-related genes (*MSX2*,[32] *SEMA5A*, *NKX2-5*,[33] *GPM6A*, *CDK6*[34] and *RBM24*) (Figure 3A). These observations again supported the idea that LAPTM4B plays an important role in regulating the stemness of HCC tumor cells. Next, Kyoto Encyclopedia of Genes and Genomes (KEGG) pathway enrichment and Gene Ontology (GO) functional category enrichment analyses revealed that the downregulated genes in the

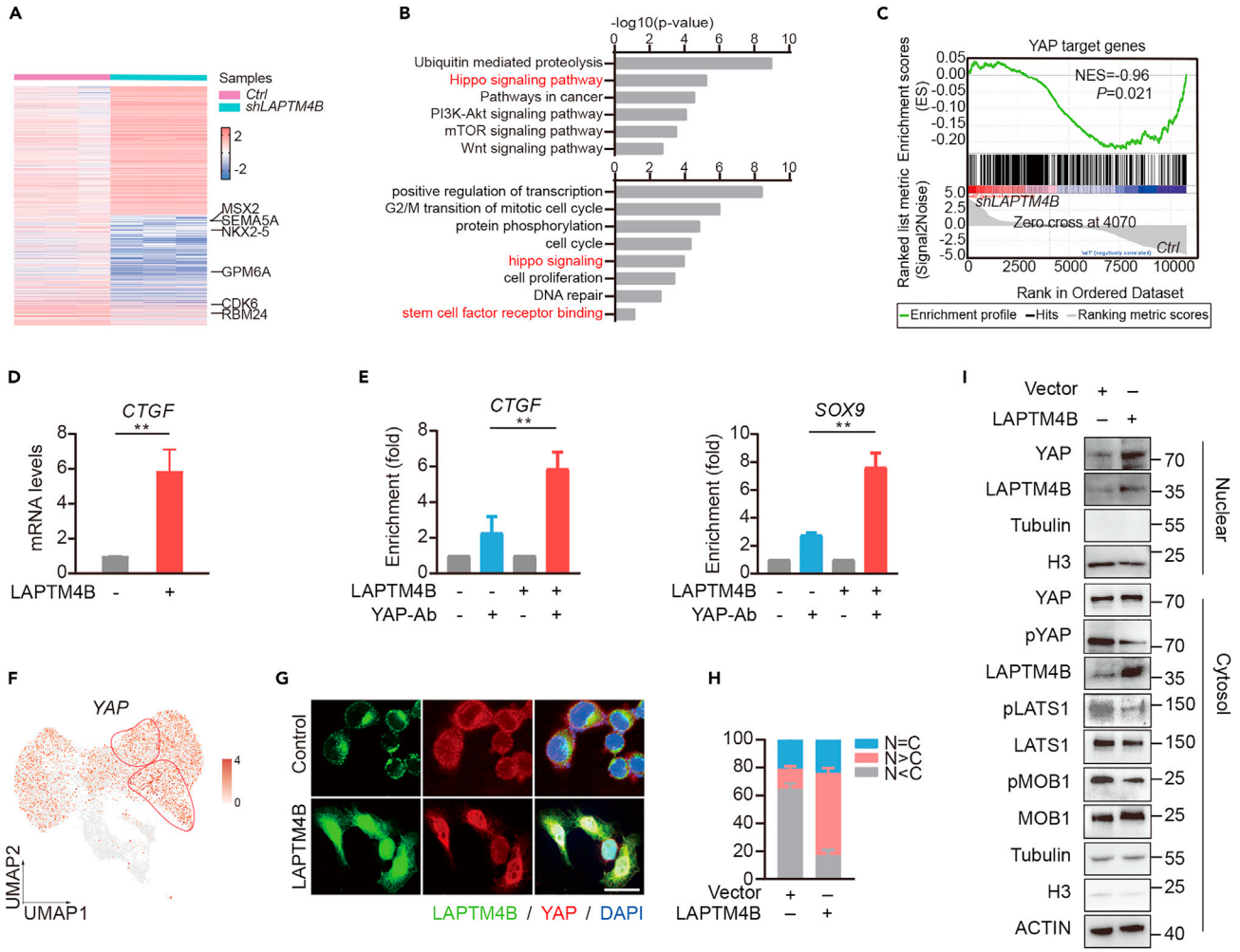

Figure 3. Effect of LAPTM4B on the transcriptional activity and nuclear localization of YAP

(A) RNA-seq transcriptional profiling of *WT* and LAPTM4B-knockdown CD133$^+$ Huh7 cells.

(B) Kyoto Encyclopedia of Genes and Genomes (KEGG) analysis and Gene Ontology (GO) of downregulated genes of LAPTM4B-knockdown CD133$^+$ Huh7 cells in Figure 3A.

(C) Gene set enrichment analysis (GSEA) showed significant negative enrichment of YAP target genes in the LAPTM4B-knockdown group.

(D) The mRNA level of *CTGF* in LAPTM4B overexpressed HepG2 cells.

(E) ChIP-qPCR experiment conducted using YAP antibody in HepG2 cells after LAPTM4B overexpression.

(F) Expression UMAP maps of YAP for tumor cells. The color bar indicates log2 normalized expression.

(G and H) Subcellular localization of YAP detected using immunofluorescence analysis. Bar, 100 μm.

(I) Nuclear localization of YAP in HepG2 cells with or without LAPTM4B-overexpressing was detected using western blotting assays. At least two independent experiments were performed for all data. For curve figures and bar figures, data are presented as means ± SD. Unpaired Student's t tests were used for comparing two variables. One-way ANOVA was used for multiple variables comparison. *, $p< 0.05$; **, $p< 0.01$; ***, $p< 0.001$; n.s., no significance in comparison with control group.

See also Figure S4.

LAPTM4B knockdown group were involved in multiple biological processes, such as ubiquitin mediated proteolysis, Hippo signaling and stem cell factor receptor binding (Figure 3B). Given the hints for the role of the Hippo signaling pathway in stemness maintenance,[17,35,36] we speculated that LAPTM4B might mediate stemness in HCC through the Hippo signaling pathway. Supporting this notion, gene set enrichment analysis (GSEA) illustrated that YAP target genes were significantly decreased in LAPTM4B silenced CD133$^+$ Huh7 cells compared with the control group (Figure 3C). Consistent results were obtained in the HepG2 cell line (Figures S4A–S4C). Compared with the control group, 1,116 genes were significantly downregulated in CD133$^+$ HepG2 cells after LAPTM4B knockdown, including some

stemness-related genes (*SEMA4B*, *SEMA3A*, *KDM3A*, *HMGA2*,[37] *SEMA3F*, *SOX9*,[26] *RUNX2*,[38] *MYB*, *SHC4*, *NRTN*, *EPCAM*,[31] *SEMA3G*, *SEMA6*) (Figure S4A). Next, Kyoto Encyclopedia of Genes and Genomes (KEGG) pathway enrichment analysis revealed that the downregulated genes in the LAPTM4B knockdown group were involved in multiple biological processes, such as protein digestion and absorption, TGF-beta signaling pathway, signaling pathways regulating pluripotency of stem cells, pathways in cancer, PI3K-Akt signaling pathway and Hippo signaling pathway (Figure S4B). In addition, compared with the control group, gene set enrichment analysis (GSEA) illustrated that the genes of Hippo pathway were significantly decreased in LAPTM4B silenced CD133$^+$ HepG2 cells (Figure S4C). Collectively, these results clearly indicate the essential role of LAPTM4B in Hippo signaling and the stemness both in Huh7 and HepG2 cells. Consistent with this result, the mRNA levels of *CTGF* and *SOX9* (known YAP target genes) were upregulated when cells overexpressed LAPTM4B (Figures 3D and S3G). Furthermore, ChIP-qPCR analysis confirmed that LAPTM4B overexpression significantly promoted YAP binding to the promoters of *CTGF* and *SOX9* (Figure 3E). These results indicated that LAPTM4B overexpression promoted the transcriptional activation of YAP. In addition, a co-expression pattern of *LAPTM4B* and *YAP* has been observed in tumor cells at the single-cell level (Figures 1J, 3F, S2A, and S4D). Given that nuclear YAP localization is associated with its transcriptional coactivator function and downstream gene activation, we observed the effect of LAPTM4B on the subcellular localization of YAP. Consistently, YAP nuclear localization was increased in LAPTM4B-overexpressing cells as detected by both immunofluorescence (Figures 3G and 3H) and nuclear/cytosol fractionation (Figure 3I). Moreover, we observed a dramatic reduction in YAP phosphorylation in the cytoplasm, whereas LATS1 (pLATS1/LATS1) and MOB1 (pMOB1/MOB1) activation was inhibited in the cytoplasm (Figure 3I). Together, these results demonstrated that a high protein level of LAPTM4B promoted the transcriptional activation and nuclear localization of YAP.

LAPTM4B stabilizes YAP by inhibiting its degradation

Phosphorylation is responsible for YAP retention in the cytoplasm for ubiquitination degradation.[39] Unsurprisingly, phosphorylated YAP (S127) was significantly reduced in HepG2 cells with overexpression of LAPTM4B, yet the total YAP protein level conversely increased (Figures 4A and 4B), suggesting that LAPTM4B might regulate the phosphorylation of YAP.

Previous studies have reported that LAPTM4B inhibits ubiquitination and degradation of proteins.[10,11] Our RNA-seq results described in Figure 3B concurred with these reports that LAPTM4B was involved in ubiquitin-mediated proteolysis. Impressively, the ubiquitinated degradation of YAP in the cytoplasm leads to poor stability and inactivated transcriptional activity.[40] Therefore, to verify the role of LAPTM4B in the stability of YAP, we applied cycloheximide (CHX) chase assays to analyze the regulation of LAPTM4B in the ubiquitinated degradation of YAP. Consistent with previous results, the protein level of YAP was lower in LAPTM4B-knockdown Huh7 cells than in the control group. The inhibitory effects were observed in the proteasome inhibitor MG132 and lysosomal inhibitor (CQ) on YAP degradation, which was attenuated by knockdown of LAPTM4B, particularly in the MG132 group (Figures 4C–4F). To further infer if LAPTM4B inhibits the ubiquitination status and subsequent degradation of YAP, we examined the MG132-treated Huh7 cells. The ubiquitination assay showed an increase in ubiquitinated YAP protein in LAPTM4B-knockdown Huh7 cells (Figure 4G). As expected, the half-life of the YAP protein was shortened in LAPTM4B-deficient cells in western blotting analysis (Figures 4H and 4I). In summary, our results implied that LAPTM4B could enhance the stability of YAP through deubiquitination.

LAPTM4B promotes stemness of stem-like tumor cells through YAP signaling

Based on our above results suggested that LAPTM4B might increase the stability and transcriptional activity of YAP by inhibiting the phosphorylation and ubiquitination degradation of YAP, we next evaluated the essential role of YAP signaling in the response to LAPTM4B in regulating the stemness of HCC tumor cells. The sphere formation assays showed that LAPTM4B overexpression promoted the sphere formation ability, whereas YAP knockdown abrogated LAPTM4B-induced sphere formation in HCC tumor cells (Figures 5A and 5B); LAPTM4B deficiency emasculated the sphere formation ability of HCC tumor cells, whereas YAP overexpression partly rescued the ability to form spheres (Figures 5C and 5D). The expressions of SOX9, EpCAM, OCT4 and NANOG were elevated when cells overexpressed LAPTM4B, and YAP depletion suppressed this upregulation in HepG2 cells (Figure 5E). In addition, we conducted limiting dilution subcutaneous xenografts of CD133$^+$ Huh7 cells and that LAPTM4B silenced CD133$^+$ Huh7 cells reduced the capacity to form tumors in immunodeficient mice, whereas overexpressing YAP effectively

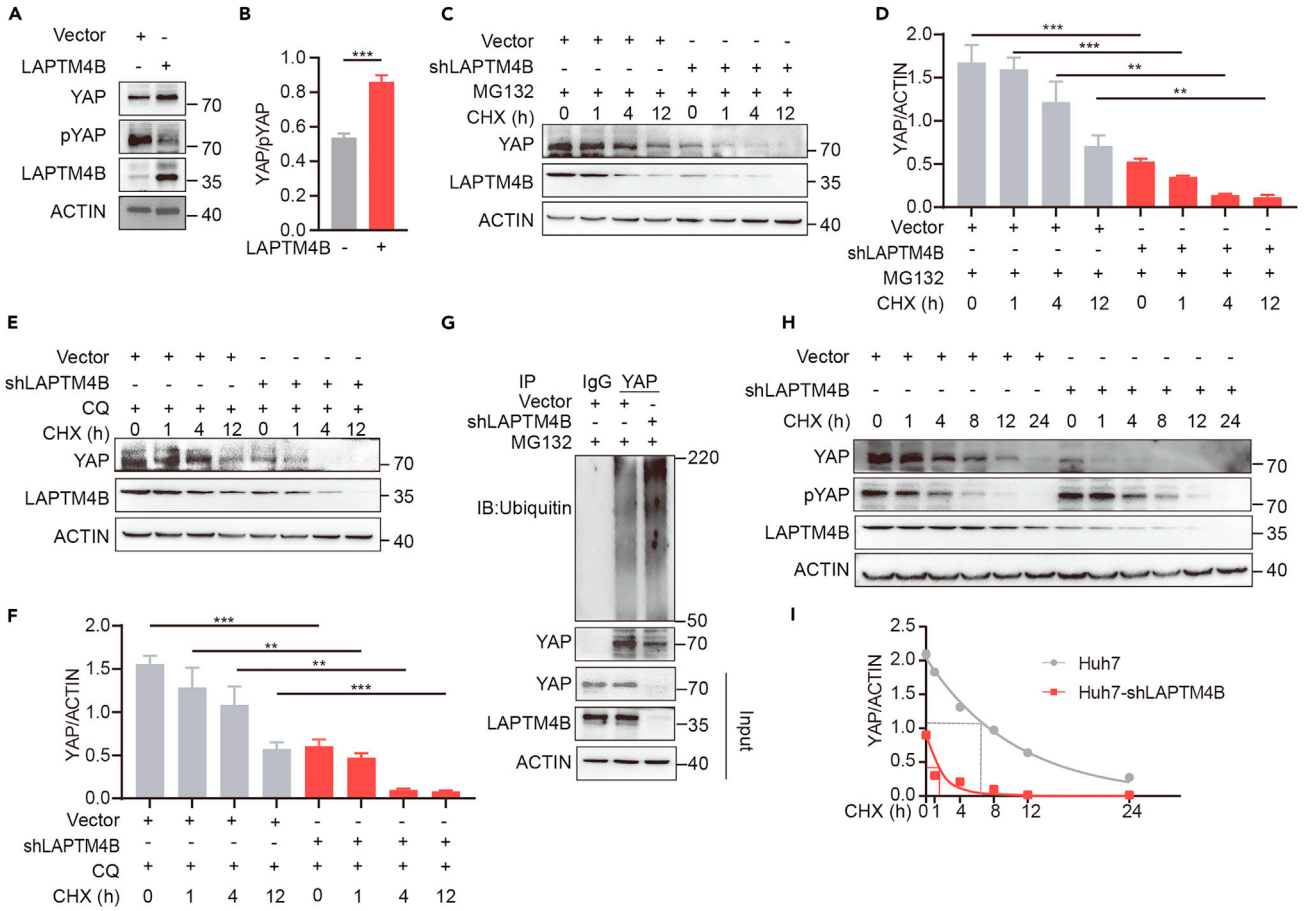

Figure 4. Effect of LAPTM4B on the degradation of YAP

(A and B) Western blotting assays detected the YAP and phosphorylated YAP protein levels of HepG2 cells with or without LAPTM4B-overexpressing.

(C and D) Western blotting was used to detect the YAP protein levels of Huh7 cells with or without LAPTM4B-knockdown after cycloheximide (CHX) and MG132 treatment.

(E and F) Western blotting was used to detect the YAP protein levels of Huh7 cells with or without LAPTM4B-knockdown after CHX and chloroquine (CQ) treatment.

(G) The *in vitro* ubiquitination assay of YAP in Huh7 cells with or without LAPTM4B-knockdown after MG132 treatment was performed and analyzed using western blotting assays.

(H and I) YAP protein and phosphorylated YAP protein levels of Huh7 cells with or without LAPTM4B-knockdown (shLAPTM4B) after CHX treatment. At least two independent experiments were performed for all data. For curve figures and bar figures, data are presented as means ± SD. Unpaired Student's t tests were used for comparing two variables. One-way ANOVA was used for multiple variables comparison. *, p< 0.05; **, p< 0.01; ***, p< 0.001; n.s., no significance in comparison with control group.

reversed LAPTM4B inhibition of tumor formation ability (Figure 5F). Together, these observations were indicative of YAP signaling increasing the role of LAPTM4B in stemness in HCC.

YAP upregulates the transcription of LAPTM4B through binding to CREB1

To clarify the role of YAP on LAPTM4B transcription, we implemented chromatin immunoprecipitation followed by sequencing (ChIP-seq) to profile the chromatin binding signatures of YAP (Figures 6A, S5A, and S5B). Subsequent integrative analysis combining genes upregulated in ChIP-seq by YAP and increased genes associated with a poor prognosis in HCC from the TCGA database identified overlapping 21 genes, including LAPTM4B (Figure 6B). Then, we further observed YAP binding at promoter regions of *LAPTM4B* and the target genes *CTGF* and *SOX9*, which was greatly enhanced following YAP overexpression (Figure 6C). In addition, both mRNA and protein of LAPTM4B increased after YAP (5SA) overexpression in HepG2 cells (Figures 6D and 6E). These results suggested the transcriptional regulation of YAP on LAPTM4B in HCC tumor cells.

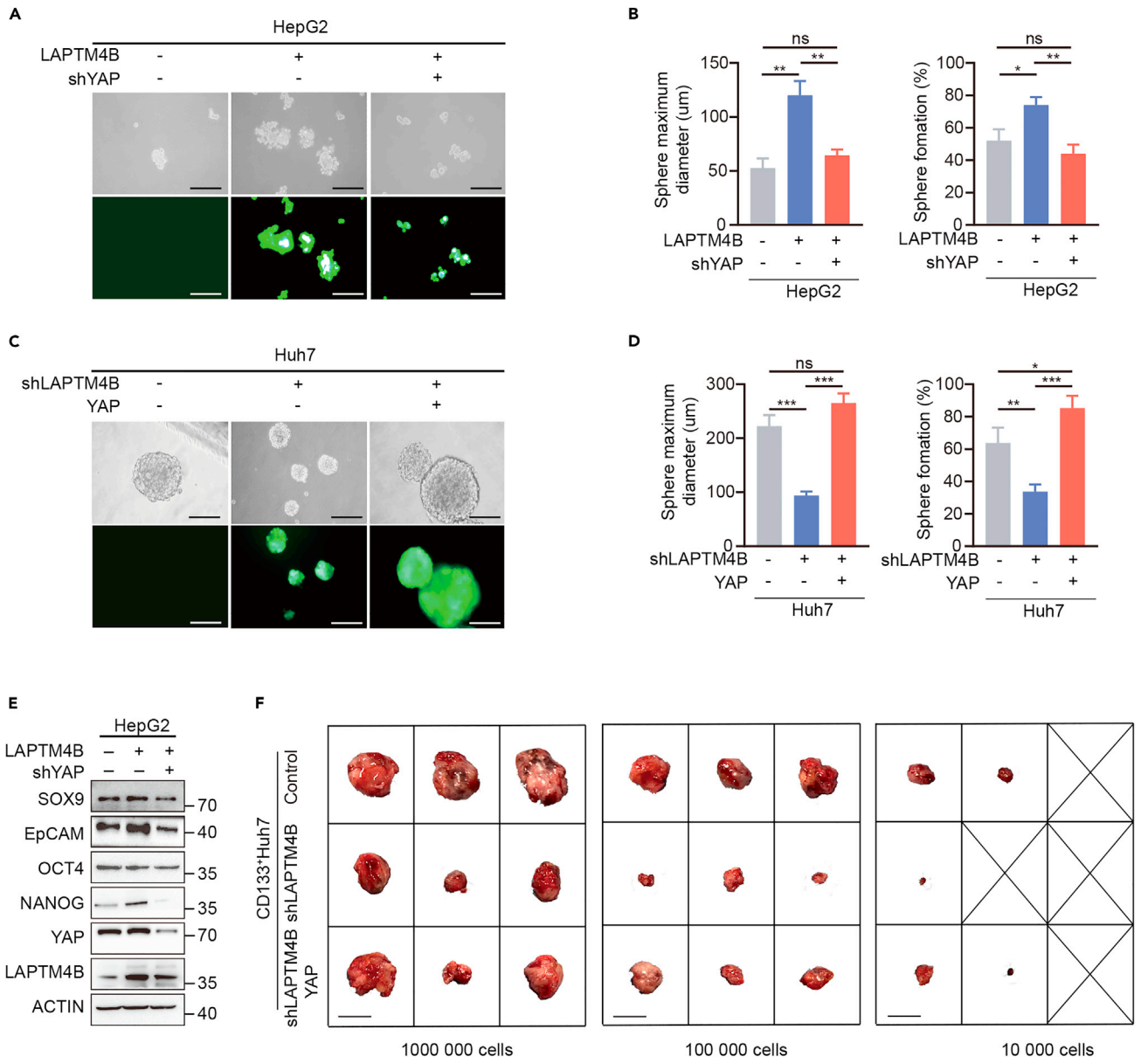

Figure 5. LAPTM4B promotes stemness via YAP-signaling in HCC

(A and B) The capacity of clones detected by sphere formation assays in LAPTM4B- overexpressing HepG2 cells with or without knockdown of YAP for 5 days. Bar, 100 μm.

(C and D) The capacity of clones detected by sphere formation assays in LAPTM4B-knockdown Huh7 cells with or without re-introduction of YAP for 5 days. Bar, 100 μm.

(E) Western blotting assays of EpCAM, NANOG, OCT4, SOX9, YAP and LAPTM4B levels in LAPTM4B-overexpressing HepG2 cells with or without knockdown of YAP.

(F) Subcutaneous xenograft assay with limited dilution detected the tumor formation ability of $CD133^{+}$Huh7 cells (n = 3 per group). At least two independent experiments were performed for all data. For curve figures and bar figures, data are presented as means ± SD. Unpaired Student's t tests were used for comparing two variables. One-way ANOVA was used for multiple variables comparison. *, $p< 0.05$; **, $p< 0.01$; ***, $p< 0.001$; n.s., no significance in comparison with control group.

CREB1 has previously been demonstrated to be a LAPTM4B transcription factor.[41] To further determine whether YAP regulates the transcription of LAPTM4B through binding to CREB1, we first mined the bioinformatics database (GeneMENIA database) to analyze potential protein-protein interactions among YAP, LAPTM4B and CREB1. Analysis of protein-protein interaction data identified there a possible link between

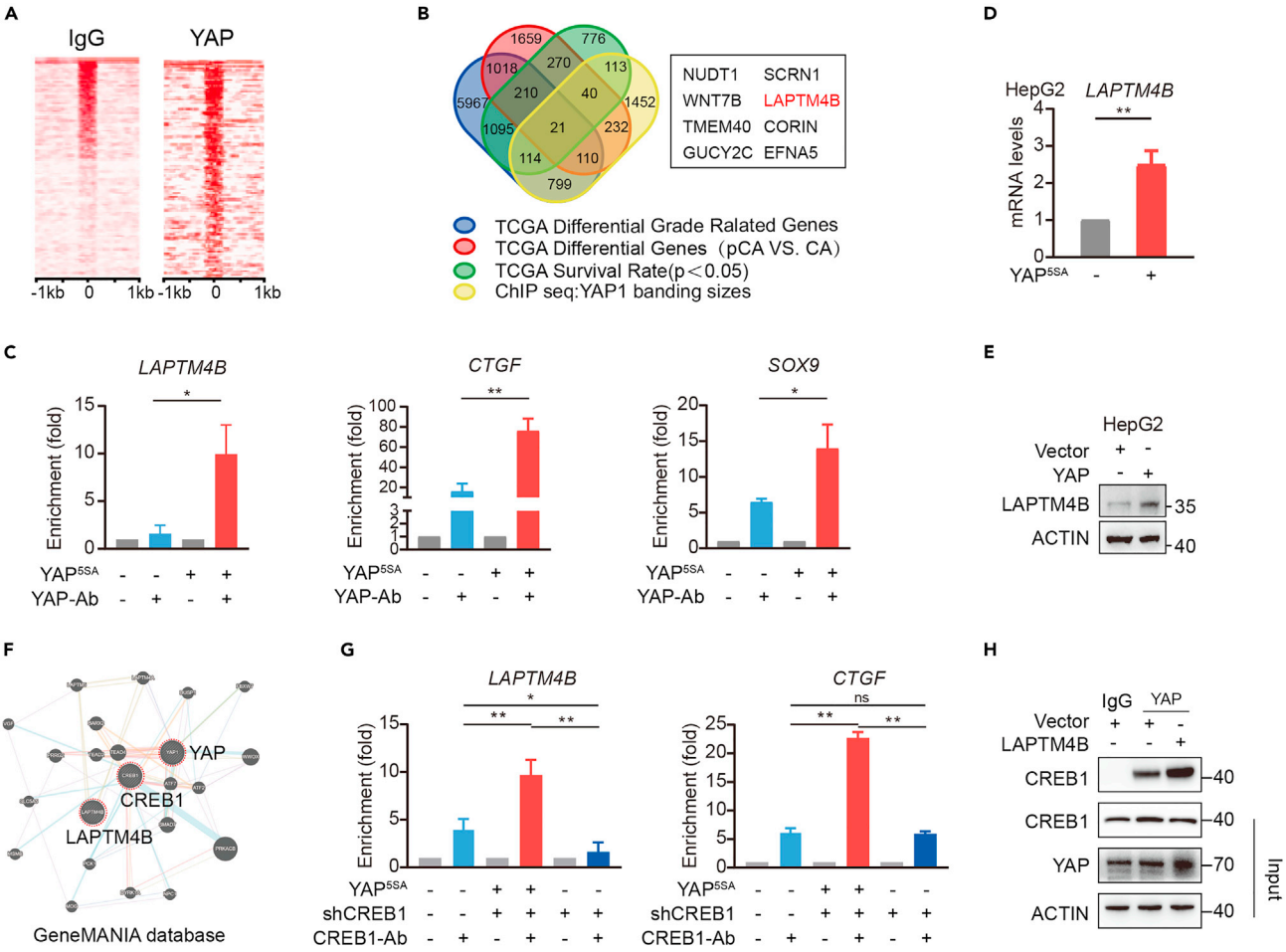

Figure 6. YAP promotes the transcription of LAPTM4B by binding to CREB1

(A) Heatmap representing IgG and YAP binding sites located on promoters.

(B) The integrative analysis combined ChIP-seqdata and a publicly available database in HCC from the TCGA database.

(C) ChIP-qPCR was performed with YAP antibody in HepG2 cells after overexpression of YAP.

(D and E) qPCR and western blotting analyses detected the expression profiles of LAPTM4B in HepG2 cells with or without YAP-overexpressing.

(F) The GeneMANIA database predicted the relationship among the YAP, CREB1 and LAPTM4B proteins.

(G) ChIP-qPCR was performed using CREB1 antibody in HepG2 cells after overexpression of YAP and knockdown of CREB1.

(H) Co-IP of YAP with CREB1 in HepG2 cells after overexpression of LAPTM4B. At least two independent experiments were performed for all data. For curve figures and bar figures, data are presented as means ± SD. Unpaired Student's *t* tests were used for comparing two variables. One-way ANOVA was used for multiple variables comparison. *, p< 0.05; **, p< 0.01; ***, p< 0.001; n.s., no significance in comparison with control group.

See also Figures S5 and S6.

YAP and CREB1, whereas the LAPTM4B protein might not directly interact with them (Figure 6F). qPCR was performed to quantitatively analyze ChIP samples using anti-CREB1 antibodies. CREB1 binding at *LAPTM4B* and *CTGF* promoter regions was notably increased after YAP overexpressing, whereas this enhancement was suppressed after CREB1 silencing (Figure 6G). Consistent with the above results, a co-IP assay confirmed the binding of YAP with CREB1 (Figure 6H). Collectively, these results indicated that YAP activated LAPTM4B transcription by binding to CREB1.

Of interest, there was a positive correlation between LAPTM4B and CREB1 (R = 0.31, p = 1.3e-109, Figure S6A). Besides, we examined the expression of CREB1 in response to LAPTM4B depletion, and found mRNA and protein levels of CREB1 were slightly decreased (Figures S6B and S6C). Thus, our data suggested that LAPTM4B protein regulated the expression of CREB1.

LAPTM4B-YAP loop feedback predicts high stemness characteristics and unfavorable prognosis in HCC patients

Based on our above results, LAPTM4B overexpression enhances the stability of YAP through inhibiting degradation. Sequencing accumulated YAP promotes LAPTM4B transcription, which forms a positive regulatory loop. To verify the correlation between LAPTM4B and YAP in HCC and the potential association of the LAPTM4B-YAP feedback loop with clinical outcomes, we assessed their expression profiles in the surgical specimens of HCC patients.

Using TCGA data, a positive correlation was found between LAPTM4B and YAP expression (R = 0.21; p = 0.00002) (Figure 7A). Consistent with this result, immunohistochemistry (IHC) analysis manifested that high protein levels of LAPTM4B appeared to be accompanied by nuclear accumulation of YAP in the tissue microarrays (TMAs) containing 73 HCC specimens with long-term clinical follow-up records (Figures 7B and 7C). A positive correlation was exhibited between the protein level of LAPTM4B and YAP ($p < 0.05$; Figure 7D and Table S1). Notably, elevated expression of LAPTM4B and YAP with increased nuclear-to-cytoplasmic ratio, more complex morphologies, and higher heterotypic structure were observed in patients 1 and 2 (Figure 7B), suggesting a link between high expression of LAPTM4B and YAP and heterogeneity of HCC patients.

Furthermore, we collected and extracted 7 available clinical factors from the patient's clinical follow-up records, the clinical background (age, sex, HBV infection and cirrhosis), and cancer stage information (tumor size, distant metastasis and tumor stage). Our results showed that LAPTM4B staining was significantly associated with age and tumor size ($p < 0.05$, Table S2) but was not significantly correlated with sex, distant metastasis, or tumor stage. YAP staining in our previous study showed that the protein level of YAP was only associated with tumor size and TNM stage ($p < 0.05$).[19]

Next, we performed a Kaplan-Meier analysis to assess the association of LAPTM4B and YAP with the overall survival of HCC patients. Our results showed a clear association between high expression levels of LAPTM4B/YAP with a poor prognosis in HCC patients (p = 0.0092, p = 0.0403) (Figures 7E and 7F). In addition, HCC patients with high levels of both LAPTM4B and YAP had shorter survival, whereas those with low levels of LAPTM4B and YAP had a longer survival (relative risk, 0.3906; 95% confidence interval, ~0.2157 to ~0.7400; p = 0.0035) (Figure 7G). Collectively, these results highlighted that the hyperactivation of LAPTM4B and YAP might be a marker of a poor prognosis in HCC patients, and demonstrated a close pathological association of this feedback loop with HCC pathogenesis.

DISCUSSION

Heterogeneity is a hallmark of hepatocellular carcinoma (HCC). Accumulating evidence has suggested that the stemness of tumor cells is essential for HCC heterogeneity and progression.[42,43] However, the molecular mechanisms underlying how cancer stem cells maintain their stemness in the complex and hostile tumor microenvironment are poorly understood and require intense investigation. Single-cell sequencing technology provides an effective tool to focus on HCC tumor stem-like cells. In the present study, lysosome-associated protein transmembrane-4β (LAPTM4B) was upregulated in stem-like cells of tumors from HCC patients at the single-cell level. Furthermore, LAPTM4B could maintain the stemness property of HCC tumor cells by forming a novel positive feedback loop with a Yes-associated protein (YAP). In addition, the combined high expression of LAPTM4B and YAP conferred a poor outcome in HCC patients.

LAPTM4B, as an oncogene, is a positive modulator in the malignant progression of HCC.[44–46] Our previous studies also confirmed that LAPTM4B can enhance the proliferation and invasion of HCC tumor cells, thereby promoting HCC progression and leading to malignant outcomes in patients.[12] However, to our best knowledge, there have hardly been any studies that demonstrated the relationship between LAPTM4B and stemness. Here, we observed a co-occurrence pattern of LAPTM4B, SOX9 and CD44 in tumor cells at the single-cell level. Our work provides evidence that LAPTM4B overexpression is associated with poor patient outcomes and can confer a high degree of stemness characteristics in HCC. This finding deepens our understanding of the impact of LAPTM4B on HCC development, allowing us to gain insight into the pathogenesis of HCC and explore individualized therapeutics.

Of note, our results suggest that LAPTM4B maintains stemness of HCC tumor cells possibly via YAP signaling. YAP, a core effector of the Hippo pathway, is involved in regulating stem cell self-renewal, proliferation and homeostasis.[17,47,48] YAP, also a transcriptional coactivator, stimulates the proliferation and expression of

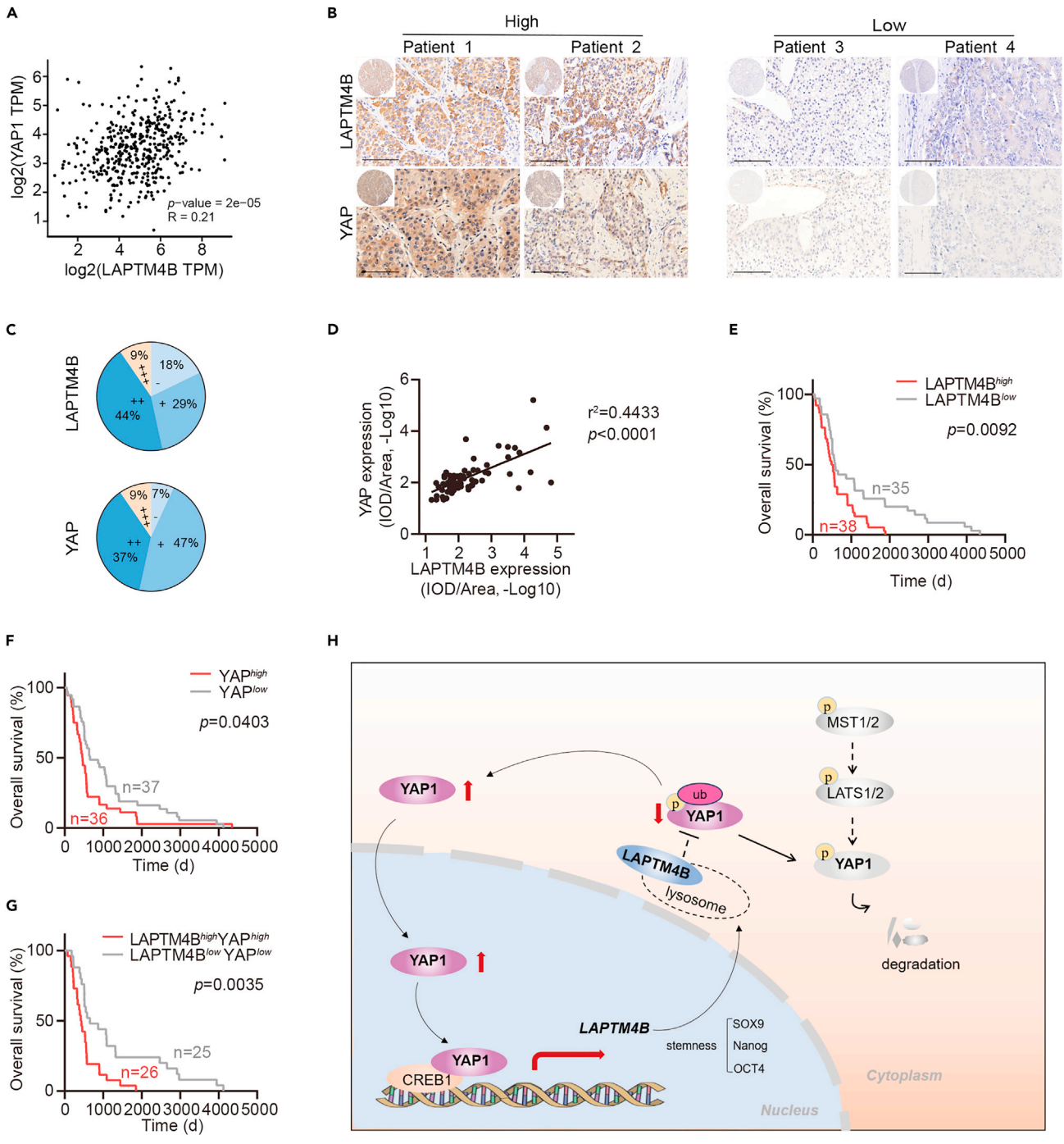

Figure 7. Pathological association of LAPTM4B with YAP in HCC

(A) Pearson's correlation analysis was used to determine the correlation between LAPTM4B and YAP in HCC patients from the TCGA database.

(B) Representative cores of LAPTM4B and YAP staining on tissue microarray. Bar, 100 μm.

(C) Staining levels of LAPTM4B and YAP in HCC tumor tissues indicate negative (–), weak (+), moderate (++), and strong (+++) expression levels.

(D) Pearson's correlation analysis determined the correlation between LAPTM4B and YAP in HCC patients.

(E) Kaplan-Meier survival analysis of patients with LAPTM4B at high or low levels using a tissue microarray.

(F) Kaplan-Meier survival analysis of patients with YAP at high or low levels using a tissue microarray.

(G) Kaplan-Meier survival analysis of patients with LAPTM4B and YAP at high or low levels using a tissue microarray.

(H) Schematic outline showing that LAPTM4B improves the stability of YAP and inhibits its degradation, whereas accumulated YAP enhances the transcription of LAPTM4B. Kaplan-Meier method was used to calculate the survival rate and Log rank test for the different significance.

cell cycle regulators and stemness-associated genes.[20,49] High levels of YAP can cause hepatocytes to sail to a progenitor-like fate.[50] Phosphorylation and ubiquitination of YAP in the cytoplasm is an important mechanism for the inhibition of YAP activity.[40,51] We further identified that LAPTM4B enhances the biological activity of YAP by inhibiting its phosphorylation and ubiquitination degradation in the cytoplasm and acting in stemness regulation in HCC, linking the phosphorylation and ubiquitination of YAP in the cytoplasm to its transition to an active functional state in the nucleus. A positive feedback loop exists between LAPTM4B and YAP, contributing to HCC stemness. In addition, considering our observations that the LAPTM4B level is positively correlated with YAP in HCC tumor specimens and that upregulated LAPTM4B and YAP levels are associated with a shorter overall survival time for HCC patients. Our work confirmed the correlation between LAPTM4B and prognosis in HCC patients that LAPTM4B with poorer prognosis/high-risk of HCC patients. Moreover, our data suggest that elevated LAPTM4B promotes the stemness of tumor cells. Mechanistically, we found that LAPTM4B impacts the activity of the key effectors of the Hippo pathway (YAP), which plays important roles in the development, tumor formation and stemness maintenance of cancer stem cells.[17,52] Targeting LAPTM4B may improve the antitumor effects in HCC by inhibiting the proliferation, invasion and stemness of tumor cells. In addition, we revealed that LAPTM4B signaling regulated YAP transcription activity, therefore pharmacological inhibitors of LAPTM4B might also antagonize Hippo pathway dysregulated tumors. Thus, LAPTM4B is an attractive potential target for HCC. Yet, it should be noted that this needs to be further evaluated by extensive clinical trials to better assess the potential target. The function of Hippo-yap signaling has been demonstrated in detail in various tumors, especially in HCC. Encouragingly, several YAP inhibitors currently under development are already in clinical trials.[53] In short, how to target this feedback loop to treat patients with HCC still needs further exploration.

In summary, this work uncovered that LAPTM4B forms a positive feedback loop with YAP, which occupies a significant position in the stemness regulation and heterogeneity formation of HCC. Briefly, our study depicts a new mechanism by which LAPTM4B inhibits YAP degradation and indirectly enhances YAP stability, thereby promoting YAP nuclear localization and transcriptional activity. The YAP accumulated in the nucleus binds to CREB1 and promotes the transcription of LAPTM4B, forming a positive feedback loop. Frequent aberrant upregulation of LAPTM4B-YAP signaling causes enhanced tumor stemness and is associated with poorer patient prognosis (Figure 7H). Our study deepens the understanding of stemness regulation in HCC and provides a potential target for individualized therapy.

Limitations of the study

We observed a significant hyperactivation of YAP in HCC tumor tissue on LAPTM4B elevated, which promotes the stemness of HCC tumor cells. Although we confirmed that LAPTM4B can inhibit the ubiquitination of YAP, enhancing its stability and increasing its nuclear accumulation. However, this study is aimed to clarify the regulation of YAP overactivation mediated by LAPTM4B, mainly through the Hippo pathway, so the intramolecular machinery regulating the YAP ubiquitination is still not well established. Also, this study indicated a positive feedback system of YAP and LAPTM4B amplification predicts a poor prognosis in HCC patients. Yet, the current study falls short of evaluating the potential target for individualized therapy of the LAPTM4B-YAP feedback loop.

STAR★METHODS

Detailed methods are provided in the online version of this paper and include the following:

- KEY RESOURCES TABLE
- RESOURCE AVAILABILITY
  - Lead contact
  - Materials availability
  - Data and code availability
- EXPERIMENTAL MODEL AND SUBJECT DETAILS
  - Cell lines
  - Reagents and antibodies
  - Animal experiments
- METHOD DETAILS
  - Single-cell dissociation
  - Single-cell sequencing
  - scRNA-seq data processing

- Cell types identification
- RNA velocity
- Isolating CD133^{+} liver cancer stem-like cells
- Sphere formation assay
- Tissue microarray and IHC staining
- Immunofluorescent staining
- Quantitative real-time polymerase chain reaction (qPCR)
- Western blotting
- ChIP-qPCR
- ChIP-seq

● QUANTIFICATION AND STATISTICAL ANALYSIS

SUPPLEMENTAL INFORMATION

Supplemental information can be found online at https://doi.org/10.1016/j.isci.2023.106754.

ACKNOWLEDGMENTS

This project was supported by National Key Program of China (Grant No. 2017YFA0504503, 2018YFA0107500), Natural Science Foundation of Fujian Province, China (Grant No. 2019J01298), National Natural Science Foundation of China (81972599, 81802737).

AUTHOR CONTRIBUTIONS

J.L., J.W., and Y.M. performed most cellular experiments and immunofluorescent assays. J.L., Q.Z., M.W., and X.T. made constructs for LAPTM4B and YAP and carried out the biochemical analysis. J.L., Y.M., and Q.Z. performed most of the ChIP-Seq and ChIP-qPCR analyses. J.L., Y.X., and Y.W. performed cellular experiments. J.L. and Y.X. packaged lentivirus. Y.M. helped with data analysis. A.H., L.W., Y.M., and J.L. designed the experiments and analyzed the data. J.L., Y.M., and A.H. wrote the manuscript. A.H. and L.W. supervised the project.

DECLARATION OF INTERESTS

The authors declare no further conflicts of interests.

INCLUSION AND DIVERSITY

We support inclusive, diverse, and equitable conduct of research.

Received: September 23, 2022
Revised: February 10, 2023
Accepted: April 23, 2023
Published: April 27, 2023

REFERENCES

1. Sung, H., Ferlay, J., Siegel, R.L., Laversanne, M., Soerjomataram, I., Jemal, A., and Bray, F. (2021). Global cancer statistics 2020: GLOBOCAN estimates of incidence and mortality worldwide for 36 cancers in 185 countries. CA. Cancer J. Clin. *71*, 209–249. https://doi.org/10.3322/caac.21660.

2. Chen, W., Zheng, R., Baade, P.D., Zhang, S., Zeng, H., Bray, F., Jemal, A., Yu, X.Q., and He, J. (2016). Cancer statistics in China, 2015. CA. Cancer J. Clin. *66*, 115–132. https://doi.org/10.3322/caac.21338.

3. Nio, K., Yamashita, T., and Kaneko, S. (2017). The evolving concept of liver cancer stem cells. Mol. Cancer *16*, 4. https://doi.org/10.1186/s12943-016-0572-9.

4. Sia, D., Villanueva, A., Friedman, S.L., and Llovet, J.M. (2017). Liver cancer cell of origin, molecular class, and effects on patient prognosis. Gastroenterology *152*, 745–761. https://doi.org/10.1053/j.gastro.2016.11.048.

5. Beck, B., and Blanpain, C. (2013). Unravelling cancer stem cell potential. Nat. Rev. Cancer *13*, 727–738. https://doi.org/10.1038/nrc3597.

6. Ling, S., Shan, Q., Zhan, Q., Ye, Q., Liu, P., Xu, S., He, X., Ma, J., Xiang, J., Jiang, G., et al. (2020). USP22 promotes hypoxia-induced hepatocellular carcinoma stemness by a HIF1alpha/USP22 positive feedback loop upon TP53 inactivation. Gut *69*, 1322–1334. https://doi.org/10.1136/gutjnl-2019-319616.

7. Liu, Y.C., Yeh, C.T., and Lin, K.H. (2020). Cancer stem cell functions in hepatocellular carcinoma and comprehensive therapeutic strategies. Cells *9*, 1331. https://doi.org/10.3390/cells9061331.

8. Liu, X., Zhou, R., Zhang, Q., Zhang, Y., Shao, G., Jin, Y., Zhang, S., Lin, M., Rui, J., and Ye, D. (2003). [Identification and characterization of LAPTM4B encoded by a human hepatocellular carcinoma-associated novel gene]. Beijing Da Xue Xue Bao Yi Xue Ban *35*, 340–347.

9. Kasper, G., Vogel, A., Klaman, I., Gröne, J., Petersen, I., Weber, B., Castaños-Vélez, E., Staub, E., and Mennerich, D. (2005). The human LAPTM4b transcript is upregulated in various types of solid tumours and seems to play a dual functional role during

tumour progression. Cancer Lett. *224*, 93–103. https://doi.org/10.1016/j.canlet.2004.10.004.

10. Shao, G.Z., Zhou, R.L., Zhang, Q.Y., Zhang, Y., Liu, J.J., Rui, J.A., Wei, X., and Ye, D.X. (2003). Molecular cloning and characterization of LAPTM4B, a novel gene upregulated in hepatocellular carcinoma. Oncogene *22*, 5060–5069. https://doi.org/10.1038/sj.onc.1206832.

11. Tan, X., Sun, Y., Thapa, N., Liao, Y., Hedman, A.C., and Anderson, R.A. (2015). LAPTM4B is a PtdIns(4,5)P2 effector that regulates EGFR signaling, lysosomal sorting, and degradation. Embo. J. *34*, 475–490. https://doi.org/10.15252/embj.201489425.

12. Su, H., Xu, T., Huang, X., Zang, S., Wang, B., Huang, Y., Liu, J., and Huang, A. (2017). Correlation of lysosome-associated protein transmembrane-4beta gene overexpression with the malignant phenotypes of hepatocellular carcinoma. Pathol. Res. Pract. *213*, 1536–1541. https://doi.org/10.1016/j.prp.2017.09.019.

13. Meng, Y., Wang, L., Chen, D., Chang, Y., Zhang, M., Xu, J.J., Zhou, R., and Zhang, Q.Y. (2016). LAPTM4B: an oncogene in various solid tumors and its functions. Oncogene *35*, 6359–6365.

14. Liu, X., Xiong, F., Wei, X., Yang, H., and Zhou, R. (2009). LAPTM4B-35, a novel tetratransmembrane protein and its PPRP motif play critical roles in proliferation and metastatic potential of hepatocellular carcinoma cells. Cancer Sci. *100*, 2335–2340. https://doi.org/10.1111/j.1349-7006.2009.01346.x.

15. Wang, J., Ma, L., Weng, W., Qiao, Y., Zhang, Y., He, J., Wang, H., Xiao, W., Li, L., Chu, Q., et al. (2013). Mutual interaction between YAP and CREB promotes tumorigenesis in liver cancer. Hepatology *58*, 1011–1020.

16. Peng, C., Zhou, R.L., Shao, G.Z., Rui, J.A., Wang, S.B., Lin, M., Zhang, S., and Gao, Z.F. (2005). Expression of lysosome-associated protein transmembrane 4B-35 in cancer and its correlation with the differentiation status of hepatocellular carcinoma. World J. Gastroenterol. *11*, 2704–2708. https://doi.org/10.3748/wjg.v11.i18.2704.

17. Ma, S., Meng, Z., Chen, R., and Guan, K.L. (2019). The Hippo pathway: biology and pathophysiology. Annu. Rev. Biochem. *88*, 577–604. https://doi.org/10.1146/annurev-biochem-013118-111829.

18. Totaro, A., Panciera, T., and Piccolo, S. (2018). YAP/TAZ upstream signals and downstream responses. Nat. Cell Biol. *20*, 888–899. https://doi.org/10.1038/s41556-018-0142-z.

19. Meng, Y., Zhao, Q., An, L., Jiao, S., Li, R., Sang, Y., Liao, J., Nie, P., Wen, F., Ju, J., et al. (2021). A TNFR2-hnRNPK Axis promotes primary liver cancer development via activation of YAP signaling in hepatic progenitor cells. Cancer Res. *81*, 3036–3050. https://doi.org/10.1158/0008-5472.CAN-20-3175.

20. Zanconato, F., Cordenonsi, M., and Piccolo, S. (2016). YAP/TAZ at the roots of cancer. Cancer Cell *29*, 783–803.

21. Zhang, S., and Zhou, D. (2019). Role of the transcriptional coactivators YAP/TAZ in liver cancer. Curr. Opin. Cell Biol. *61*, 64–71. https://doi.org/10.1016/j.ceb.2019.07.006.

22. Chen, M., Wu, L., Tu, J., Zhao, Z., Fan, X., Mao, J., Weng, Q., Wu, X., Huang, L., Xu, M., and Ji, J. (2018). miR-590-5p suppresses hepatocellular carcinoma chemoresistance by targeting YAP1 expression. EBioMedicine *35*, 142–154. https://doi.org/10.1016/j.ebiom.2018.08.010.

23. Liu, Y., Zhuo, S., Zhou, Y., Ma, L., Sun, Z., Wu, X., Wang, X.W., Gao, B., and Yang, Y. (2022). Yap-Sox9 signaling determines hepatocyte plasticity and lineage-specific hepatocarcinogenesis. J. Hepatol. *76*, 652–664. https://doi.org/10.1016/j.jhep.2021.11.010.

24. Meng, Y., Sang, Y., Liao, J., Zhao, Q., Qu, S., Li, R., Jiang, J., Wang, M., Wang, J., Wu, D., et al. (2022). Single cell transcriptional diversity and intercellular crosstalk of human liver cancer. Cell Death Dis. *13*, 261.

25. Becht, E., McInnes, L., Healy, J., Dutertre, C.A., Kwok, I.W.H., Ng, L.G., Ginhoux, F., and Newell, E.W. (2018). Dimensionality reduction for visualizing single-cell data using UMAP. Nat. Biotechnol. *37*, 38–44. https://doi.org/10.1038/nbt.4314.

26. Guo, W., Keckesova, Z., Donaher, J.L., Shibue, T., Tischler, V., Reinhardt, F., Itzkovitz, S., Noske, A., Zürrer-Härdi, U., Bell, G., et al. (2012). Slug and Sox9 cooperatively determine the mammary stem cell state. Cell *148*, 1015–1028. https://doi.org/10.1016/j.cell.2012.02.008.

27. Müller, S., Sindikubwabo, F., Cañeque, T., Lafon, A., Versini, A., Lombard, B., Loew, D., Wu, T.D., Ginestier, C., Charafe-Jauffret, E., et al. (2020). CD44 regulates epigenetic plasticity by mediating iron endocytosis. Nat. Chem. *12*, 929–938. https://doi.org/10.1038/s41557-020-0513-5.

28. Suetsugu, A., Nagaki, M., Aoki, H., Motohashi, T., Kunisada, T., and Moriwaki, H. (2006). Characterization of CD133+ hepatocellular carcinoma cells as cancer stem/progenitor cells. Biochem. Biophys. Res. Commun. *351*, 820–824. https://doi.org/10.1016/j.bbrc.2006.10.128.

29. Zhang, C., Huang, S., Zhuang, H., Ruan, S., Zhou, Z., Huang, K., Ji, F., Ma, Z., Hou, B., and He, X. (2020). YTHDF2 promotes the liver cancer stem cell phenotype and cancer metastasis by regulating OCT4 expression via m6A RNA methylation. Oncogene *39*, 4507–4518. https://doi.org/10.1038/s41388-020-1303-7.

30. Chen, C.L., Uthaya Kumar, D.B., Punj, V., Xu, J., Sher, L., Tahara, S.M., Hess, S., and Machida, K. (2016). NANOG metabolically reprograms tumor-initiating stem-like cells through tumorigenic changes in oxidative phosphorylation and fatty acid metabolism. Cell Metab. *23*, 206–219.

31. Park, D.J., Sung, P.S., Kim, J.H., Lee, G.W., Jang, J.W., Jung, E.S., Bae, S.H., Choi, J.Y., and Yoon, S.K. (2020). EpCAM-high liver cancer stem cells resist natural killer cell-mediated cytotoxicity by upregulating CEACAM1. J. Immunother. Cancer *8*, e000301. https://doi.org/10.1136/jitc-2019-000301.

32. Inada, E., Saitoh, I., Kubota, N., Soda, M., Matsueda, K., Murakami, T., Sawami, T., Kagoshima, A., Yamasaki, Y., and Sato, M. (2017). Alkaline phosphatase and OCT-3/4 as useful markers for predicting susceptibility of human deciduous teeth-derived dental pulp cells to reprogramming factor-induced iPS cells. J. Investig. Clin. Dent. *8*, e12236. https://doi.org/10.1111/jicd.12236.

33. Ghiasi, P., Hosseinkhani, S., Ansari, H., Aghdami, N., Balalaei, S., Pahlavan, S., and Baharvand, H. (2018). Reversible permeabilization of the mitochondrial membrane promotes human cardiomyocyte differentiation from embryonic stem cells. J. Cell. Physiol. *234*, 521–536. https://doi.org/10.1002/jcp.26758.

34. Ho, C.M., Chang, T.H., Yen, T.L., Hong, K.J., and Huang, S.H. (2021). Collagen type VI regulates the CDK4/6-p-Rb signaling pathway and promotes ovarian cancer invasiveness, stemness, and metastasis. Am. J. Cancer Res. *11*, 668–690.

35. Wang, T., Qin, Z.Y., Wen, L.Z., Guo, Y., Liu, Q., Lei, Z.J., Pan, W., Liu, K.J., Wang, X.W., Lai, S.J., et al. (2018). Epigenetic restriction of Hippo signaling by MORC2 underlies stemness of hepatocellular carcinoma cells. Cell Death Differ. *25*, 2086–2100. https://doi.org/10.1038/s41418-018-0095-6.

36. Basu-Roy, U., Bayin, N.S., Rattanakorn, K., Han, E., Placantonakis, D.G., Mansukhani, A., and Basilico, C. (2015). Sox2 antagonizes the Hippo pathway to maintain stemness in cancer cells. Nat. Commun. *6*, 6411. https://doi.org/10.1038/ncomms7411.

37. Mansoori, B., Duijf, P.H., Mohammadi, A., Najafi, S., Roshani, E., Shanehbandi, D., Hajiasgharzadeh, K., Shirjang, S., Ditzel, H.J., Kazemi, T., et al. (2020). Overexpression of HMGA2 in breast cancer promotes cell proliferation, migration, invasion and stemness. Expert Opin. Ther. Targets *24*, 255–265. https://doi.org/10.1080/14728222.2020.1736559.

38. Saito, K., Takahashi, K., Huang, B., Asahara, M., Kiso, H., Togo, Y., Tsukamoto, H., Mishima, S., Nagata, M., Iida, M., et al. (2018). Loss of stemness, EMT, and supernumerary tooth formation in Cebpb(-/-)Runx2(+/-) murine incisors. Sci. Rep. *8*, 5169. https://doi.org/10.1038/s41598-018-23515-y.

39. Dey, A., Varelas, X., and Guan, K.L. (2020). Targeting the Hippo pathway in cancer, fibrosis, wound healing and regenerative medicine. Nat. Rev. Drug Discov. *19*, 480–494. https://doi.org/10.1038/s41573-020-0070-z.

40. Ni, W., Yao, S., Zhou, Y., Liu, Y., Huang, P., Zhou, A., Liu, J., Che, L., and Li, J. (2019). Long noncoding RNA GAS5 inhibits progression of colorectal cancer by interacting with and triggering YAP phosphorylation and

degradation and is negatively regulated by the m(6)A reader YTHDF3. Mol. Cancer *18*, 143. https://doi.org/10.1186/s12943-019-1079-y.

41. Zhang, M., Xu, J.J., Zhou, R.L., and Zhang, Q.Y. (2013). cAMP responsive element binding protein-1 is a transcription factor of lysosomal-associated protein transmembrane-4 beta in human breast cancer cells. PLoS One *8*, e57520.

42. Sell, S., and Leffert, H.L. (2008). Liver cancer stem cells. J. Clin. Oncol. *26*, 2800–2805. https://doi.org/10.1200/JCO.2007.15.5945.

43. Zhi, X.S., Xiong, J., Zi, X.Y., and Hu, Y.P. (2016). The potential role of liver stem cells in initiation of primary liver cancer. Hepatol. Int. *10*, 893–901. https://doi.org/10.1007/s12072-016-9730-9.

44. Meng, Y., Wang, L., Xu, J., and Zhang, Q. (2018). AP4 positively regulates LAPTM4B to promote hepatocellular carcinoma growth and metastasis, while reducing chemotherapy sensitivity. Mol. Oncol. *12*, 373–390. https://doi.org/10.1002/1878-0261.12171.

45. Li, L., Shan, Y., Yang, H., Zhang, S., Lin, M., Zhu, P., Chen, X.Y., Yi, J., McNutt, M.A., Shao, G.Z., and Zhou, R.L. (2011). Upregulation of LAPTM4B-35 promotes malignant transformation and tumorigenesis in L02 human liver cell line. Anat. Rec. *294*, 1135–1142. https://doi.org/10.1002/ar.21421.

46. Yang, H., Xiong, F., Qi, R., Liu, Z., Lin, M., Rui, J., Su, J., and Zhou, R. (2010). LAPTM4B-35 is a novel prognostic factor of hepatocellular carcinoma. J. Surg. Oncol. *101*, 363–369. https://doi.org/10.1002/jso.21489.

47. Zheng, Y., and Pan, D. (2019). The Hippo signaling pathway in development and disease. Dev. Cell *50*, 264–282. https://doi.org/10.1016/j.devcel.2019.06.003.

48. Yu, F.X., Zhao, B., and Guan, K.L. (2015). Hippo pathway in organ size control, tissue homeostasis, and cancer. Cell *163*, 811–828. https://doi.org/10.1016/j.cell.2015.10.044.

49. Zhang, Z., Du, J., Wang, S., Shao, L., Jin, K., Li, F., Wei, B., Ding, W., Fu, P., van Dam, H., et al. (2019). OTUB2 promotes cancer metastasis via hippo-independent activation of YAP and TAZ. Mol. Cell *73*, 7–21.e7. https://doi.org/10.1016/j.molcel.2018.10.030.

50. Yimlamai, D., Christodoulou, C., Galli, G.G., Yanger, K., Pepe-Mooney, B., Gurung, B., Shrestha, K., Cahan, P., Stanger, B.Z., and Camargo, F.D. (2014). Hippo pathway activity influences liver cell fate. Cell *157*, 1324–1338. https://doi.org/10.1016/j.cell.2014.03.060.

51. Yao, F., Zhou, Z., Kim, J., Hang, Q., Xiao, Z., Ton, B.N., Chang, L., Liu, N., Zeng, L., Wang, W., et al. (2018). SKP2- and OTUD1-regulated non-proteolytic ubiquitination of YAP promotes YAP nuclear localization and activity. Nat. Commun. *9*, 2269. https://doi.org/10.1038/s41467-018-04620-y.

52. Han, Y. (2019). Analysis of the role of the Hippo pathway in cancer. J. Transl. Med. *17*, 116. https://doi.org/10.1186/s12967-019-1869-4.

53. Pobbati, A.V., and Hong, W. (2020). A combat with the YAP/TAZ-TEAD oncoproteins for cancer therapy. Theranostics *10*, 3622–3635. https://doi.org/10.7150/thno.40889.

54. Hafemeister, C., and Satija, R. (2019). Normalization and variance stabilization of single-cell RNA-seq data using regularized negative binomial regression. Genome Biol. *20*, 296.

55. Ma, L., Hernandez, M.O., Zhao, Y., Mehta, M., Tran, B., Kelly, M., Rae, Z., Hernandez, J.M., Davis, J.L., Martin, S.P., et al. (2019). Tumor cell biodiversity drives microenvironmental reprogramming in liver cancer. Cancer Cell *36*, 418–430.e6. https://doi.org/10.1016/j.ccell.2019.08.007.

56. Zong, C., Lu, S., Chapman, A.R., and Xie, X.S. (2012). Genome-wide detection of single-nucleotide and copy-number variations of a single human cell. Science *338*, 1622–1626. https://doi.org/10.1126/science.1229164.

57. Zheng, C., Zheng, L., Yoo, J.K., Guo, H., Zhang, Y., Guo, X., Kang, B., Hu, R., Huang, J.Y., Zhang, Q., et al. (2017). Landscape of infiltrating T cells in liver cancer revealed by single-cell sequencing. Cell *169*, 1342–1356.e16. https://doi.org/10.1016/j.cell.2017.05.035.

58. Zhang, Q., He, Y., Luo, N., Patel, S.J., Han, Y., Gao, R., Modak, M., Carotta, S., Haslinger, C., Kind, D., et al. (2019). Landscape and dynamics of single immune cells in hepatocellular carcinoma. Cell *179*, 829–845.e20. https://doi.org/10.1016/j.cell.2019.10.003.

59. Massalha, H., Bahar Halpern, K., Abu-Gazala, S., Jana, T., Massasa, E.E., Moor, A.E., Buchauer, L., Rozenberg, M., Pikarsky, E., Amit, I., et al. (2020). A single cell atlas of the human liver tumor microenvironment. Mol. Syst. Biol. *16*, e9682. https://doi.org/10.15252/msb.20209682.

60. Nelson, J.D., Denisenko, O., and Bomsztyk, K. (2006). Protocol for the fast chromatin immunoprecipitation (ChIP) method. Nat. Protoc. *1*, 179–185. https://doi.org/10.1038/nprot.2006.27.

STAR★METHODS

KEY RESOURCES TABLE

REAGENT or RESOURCE	SOURCE	IDENTIFIER
Antibodies		
Phospho-YAP (Ser127) (D9W2I) Rabbit mAb	Cell Signaling Technology	Cat# 13008; RRID: AB_2650553
α-Tubulin Antibody	Cell Signaling Technology	Cat# 2144; RRID: AB_2210548
CREB (48H2) Rabbit mAb	Cell Signaling Technology	Cat# 9197; RRID: AB_331277
YAP (D8H1X) XP®Rabbit mAb	Cell Signaling Technology	Cat# 14729; RRID: AB_2798588
YAP1 antibody (63.7)	Santa Cruz Biotechnology	Cat# sc-101199; RRID: AB_1131430
Anti-EpCAM antibody	Abcam	Cat# ab71916; RRID: AB_1603782
Recombinant Anti-SOX9 antibody [EPR14335]	Abcam	Cat# ab185230; RRID: AB_2715497
Anti-LAPTM4B antibody	Abcam	Cat# ab82810; RRID: AB_1860804
Anti-Nanog antibody	Abcam	Cat# ab14959; RRID: AB_443111
Recombinant Anti-YAP1 (phospho S127) antibody [EP1675Y]	Abcam	Cat# ab76252; RRID: AB_1524578
Anti-Oct4 antibody	Abcam	Cat# ab19857; RRID: AB_445175
Flag antibodies	Sigma-Aldrich	Cat# F3165; RRID: AB_259529
Bacterial and virus strains		
LV3 (H1/GFP&Puro)vector	GenePharma	N/A
LV-LAPTM4B	HANBI	N/A
Biological samples		
HCC tumor tissue	Shanghai Outdo Biotech Co. Ltd	N/A
Chemicals, peptides, and recombinant proteins		
Collagenase II	Thermo Fisher	Cat# 17101015
red blood cell lysis buffer	Miltenyi Biotec	Cat# 130-094-183
basic fibroblast growth factor (bFGF)	Peprotech	Cat# AF-100-18B
epidermal growth factor (EGF)	Peprotech	Cat# AF-100-15
Triton X-100	Beyotime	Cat# ST795
Na-deoxycholate	MACKLIN	Cat# S817543
protease inhibitors	MCE	Cat# HY-K0010
Chelex	Bio-Rad	Cat# 1421253
Critical commercial assays		
MACS dead cell removal kit	Miltenyi Biotec	Cat# 130-090-101
Qubit High Sensitivity DNA assay	Thermo Fisher Scientific	Cat# Q33231
PrimeScript RT reagent kit	Takara Bio	Cat# RR037A
PCR purification kit	Sangon Biotech	Cat# B518141
Deposited data		
Raw and analyzed data	This paper	GSE229205, GSE218561, GSE166627
Experimental models: Cell lines		
Human: Huh7 cell	National Collection of Authenticated Cell Cultures	CSTR:19375.09.3101HUMSCSP526
Human: HepG2 cell	Procell	PC-H2022092002
Human: $CD133^+$ HCC tumor cells	Isolating from Huh7 and HepG2 cells	N/A

(*Continued on next page*)

Continued

REAGENT or RESOURCE	SOURCE	IDENTIFIER
Experimental models: Organisms/strains		
Mouse: BALB/c male nude mice (3–5 weeks, 20-25g)	Shanghai Experimental Center, Chinese Science Academy	N/A
Oligonucleotides		
Primers for XX, see "quantitative real-time polymerase chain reaction (qPCR)"	This paper	N/A
Recombinant DNA		
Plasmid: GFP-Puro	This paper	N/A
Software and algorithms		
SPSS software version 22.0	Chicago	https://www.ibm.com/support/pages/spss-statistics-220-available-download
scvelo's transition_matrix function	Miniconda	https://scvelo.readthedocs.io/getting_started/
Seurat package (version 3.0)	Hafemeister C and Satija R[54]	https://satijalab.org/seurat/
velocyto python package	Ma et al.[55] Zong et al.[56]	http://velocyto.org/velocyto.py/tutorial/analysis.html
ImageJ	National Institutes of Health (NIH)	https://imagej.nih.gov/ij/

RESOURCE AVAILABILITY

Lead contact

Further information and requests for resources and reagents should be directed to and will be fulfilled by the lead contact, Aimin Huang (aimin@fjmu.edu.cn).

Materials availability

All materials used in this study are either commercially available or through collaboration, as indicated.

Data and code availability

- The RNA-seq data can be found at the following GEO accession number: GSE229205. The scRNA-seq data can be found at the following GEO accession number: GSE218561 and GSE166627.
- This paper does not report original code.
- Any additional information required to reanalyze the data reported in this paper is available from the lead contact upon request.

EXPERIMENTAL MODEL AND SUBJECT DETAILS

Cell lines

HCC cell lines (Huh7 and HepG2) were purchased from National Collection of Authenticated Cell Cultures and Procell, and cultured in DMEM media (Gibco) with Fetal Bovine Serum (FBS, 10%; Gibco) and Penicillin-Streptomycin (100 U; Gibco) at 37°C, 5% CO2.

Reagents and antibodies

Antibodies specific for pYAP-S127 (13008), α-tubulin (2144s), CREB (9197) and YAP (14074, WB) were purchased from Cell Signaling Technology (MA); YAP (sc-101199, IF/ChIP/Co-IP) were purchased from Santa Cruz Biotechnology (TX); and EpCAM (ab71916), SOX9 (ab185230), LAPTM4B (ab82810, WB/IF/IHC), Nanog (ab14959), pYAP (ab76252) and OCT4 (ab19857) were from Abcam (MA).

Animal experiments

Male nude mice (3–5 weeks, 20-25g) were purchased from Shanghai Experimental Center, Chinese Science Academy, Shanghai. The mice were housed under pathogen-free conditions. All animals' experiments were according to the animal protocols approved by the Shanghai Eastern Hepatobiliary Surgery Hospital

Animal Care Committee. For subcutaneous inoculation, 5×10^6 cells were injected. Animals were sacrificed and the incidence and volume of subcutaneous tumors were monitored.

METHOD DETAILS

Single-cell dissociation

The tissue samples were processed as described below.[57] Briefly, samples were first washed with PBS, minced into small pieces (approximately 1 mm^3) on ice and enzymatically digested with 1 mg/mL collagenase II (Worthington) for 30 min at 37°C, with agitation. After digestion, samples were sieved through a 70 μm cell strainer, and centrifuged at 300g for 5 min. After the supernatant was removed, the pelleted cells were suspended in red blood cell lysis buffer (Miltenyi Biotec) to lyse red blood cells. After washing with PBS containing 0.04% BSA, the cell pellets were resuspended in PBS containing 0.04% BSA and re-filtered through a 35 μm cell strainer. Dissociated single cells were then stained with AO/PI for viability assessment using Countstar Fluorescence Cell Analyzer. The single-cell suspension was further enriched with a MACS dead cell removal kit (Miltenyi Biotec).

Single-cell sequencing

The scRNA-Seq libraries were generated using the 10X Genomics Chromium Controller Instrument and Chromium Single Cell 3′ V3 Reagent Kits (10X Genomics, Pleasanton, CA).[58] Briefly, the cell concentration was adjusted to 1000 cells/uL. Then, the single-cell Gel Bead-In-Emulsions (GEMs) were generated after loading more than 8,000 cells into each channel. Barcoded-cDNA was purified and amplified in the RT step after breaking the GEMs. The amplified barcoded cDNA was modified (Fragmentation, A-tailing, and linking with adaptors) and index PCR amplified. The final libraries were quantified and were analyzed the size distribution by the Qubit High Sensitivity DNA assay (Thermo Fisher Scientific) and a High Sensitivity DNA chip on a Bioanalyzer 2200 (Agilent). Subsequently, all libraries were sequenced using HiSeq Xten (Illumina, San Diego, CA).

scRNA-seq data processing

scRNA-seq data of tumor samples (n = 4) were filtered (both gene and cell) and normalized by performing the Seurat package (version 3.0)[54] in R (version 3.5.3). The genes were removed which were expressed in less than 3 cells. The cells expressing less than 500 genes or mitochondrial gene content >20% of the total UMI count were also excluded. After normalizing the total number of transcripts for all single cells to 10,000, the genes whose average expression level was between 0.05 and 3 and the dispersion was greater than 0.5 were defined as highly variable genes. Those variable genes were further used for PCA.[55]

Cell types identification

We performed data scaling based on variable genes across cells, followed by dimension reduction with PCA. The first 20 PCAs are used to show different single-cell subpopulations in the UMAP plot. We compared the known cell lineage-specific marker genes and annotated the cells as T cells (CD4, CD3E, CD3D, CD3G, CD8A, CD8B), B cells (BLNK, CD79A, FCRL5, SLAMF7), LECs (PECAM1, VWF, ENG, CDH5), Monocytes (FCN1, VCAN), Fibroblasts (COL1A2, FAP, ACTA1, COL3A1, COL6A1), Macrophages (CD14, CD163, CD68, CSF1R) and tumor cells (AFP, ALB, HP, EPCAM).[55,59]

RNA velocity

To conduct the RNA velocity analysis, the velocyto python package was applied to annotate the reads based on bam files.[55,56] The RNA velocity value of each gene of all single cells was calculated, and the RNA velocity vector was embedded in the low-dimensional space employing the scvelo python pipeline. To infer the internal migration direction of tumor cells, we constructed a partition-based map abstraction of tumor cell subpopulations, and analyzed the migration between tumor cell subpopulations according to the transition matrix of cell RNA velocity (calculated by scvelo's transition_matrix function).

Isolating $CD133^+$ liver cancer stem-like cells

To isolate and purity $CD133^+$ HCC tumor cells, we digested adherent cells (HepG2 and Huh7 HCC cell lines) (trypsin, 37 °C, 3 min) to prepare cell suspension. Then, $CD133^+$ cells were isolated using immunomagnetic beads. The obtained cells were cultured with the conditioned medium in ultra-low adsorption culture dishes. The conditioned medium was serum-free and contained DMEM/F12, 100 IU/mL penicillin

G and 100 μg/mL streptomycin (Sigma, USA), 20 ng/mL basic fibroblast growth factor (bFGF) and epidermal growth factor (EGF) (Peprotech, USA).

Sphere formation assay

① Sphere-formation assay was performed ultra-low adsorption 6-well culture plate. Cells were incubated in serum-free medium at a density of 2000 cells/well for 5 days. The numbers and size of the sphere were measured under a microscope. ② Cells were seeded at limiting dilution into 96-well plates with a density from 1 to 64 cell(s)/well and cultured for 5 days. The numbers and size of the sphere were measured under a microscope.

Tissue microarray and IHC staining

HCC tumor tissue microarray (TMA) sections were fabricated by Shanghai Outdo Biotech Co. Ltd. (Shanghai, China). After excluding patients who received local or systemic treatment before surgery, 77 fresh HCC tumor tissues were included in the TMA. For IHC, the expression profiles of LAPTM4B and YAP were examined with anti-LAPTM4B antibody (1:100 dilution) and anti-YAP antibody (1:200 dilution). The stains were interpreted by two independent pathologists who were blinded to the patients. The score is equal to the staining intensity multiplied by the extent: the staining intensity was classified as 0–3, representing negative, weak, moderate and strong, respectively; staining extent was scored as 0–4 according to the percentage of positive cells (<5%, 5–25%, 26–50%, 51–75% and >75%). Thus, the IHC result was classified as 0–1, negative (−); 2–4, weakly positive (+); 5–8, moderately positive (++), and 9–12, strongly positive (+++).

Immunofluorescent staining

For antigen colocalization studies, double-fluorescence immunostaining of paraffin-embedded tissue was performed with a sequential fluorescent method. The primary antibodies of anti-LAPTM4B antibody (1:50 dilution) and anti-YAP antibody (1:100 dilution) were used. Alexa 561-conjugated goat anti-mouse IgG (Invitrogen, Carlsbad, CA), Alexa 488-conjugated goat anti-rabbit IgG (Invitrogen) were used as secondary antibodies.

Quantitative real-time polymerase chain reaction (qPCR)

Total RNAs were extracted from cells by using Trizol Reagent (Invitrogen, Carlsbad, CA, USA). RT was performed with the PrimeScript RT reagent kit (Takara Bio, Tokyo, Japan) according to the manufacturer's protocol. qPCR was performed by the Light Cycler 480 system (Roche Diagnostics, Mannheim, Germany). The primers were used in this experiment:

Primer		Sequence (5′ → 3′)
h*CYR61* (ChIP)	Forward	AACTTGCCTCTCACCTTCGC
	Reverse	GTTTGGTGATGCGAGTTGACC
h*CTGF* (ChIP)	Forward	ACAGGGACATTCCTCGCATT
	Reverse	TGAATCAGGAGTGGTGCGAA
h*LAPTM4B 1* (ChIP)	Forward	GATCAGAAACGCAGGGGACA
	Reverse	CGAGGAGTACAGTGCAGTGAAG
h*LAPTM4B 3* (ChIP)	Forward	GACAGCCCCCTATCGACTTC
	Reverse	CAAACTCGTTGACATCGAAGG
h*LAPTM4B 5* (ChIP)	Forward	GAGTTACACGAACGGCCAGA
	Reverse	CCAAGCACCCGGTGAGTAAA
h*YAP1*	Forward	CAAATTCTCCAAAATGTCAGGAGTT
	Reverse	AAGGATCTGAGCTATTGGTCGTC
h*LAPTM4B*	Forward	GACGCGGTTCTACTCCAACAGC
	Reverse	TCAGATACCAGACGCCGAGCAG

(*Continued on next page*)

Continued

Primer		Sequence (5′→3′)
h*EpCAM*	Forward	GTCTGTGAAAACTACAAGCTGG
	Reverse	CAGTATTTTGTGCACCAACTGA
h*NANOG*	Forward	GCCTCCAGCAGATGCAAGAACTC
	Reverse	CCAGGTCTGGTTGCTCCACATTG
h*OCT4*	Forward	GATGTGGTCCGAGTGTGGTTC
	Reverse	CGAGGAGTACAGTGCAGTGAAG
h*CTGF*	Forward	TTGACCAGACTGGCGCTCTC
	Reverse	GTGCACCATCTTTGGCAGTG

Western blotting

Protein samples were extracted and equivalent aliquots of protein were electrophoresed on a 10% SDS/polyacrylamide gel and transferred to polyvinylidene membranes. Then the membranes were incubated with primary antibodies overnight at 4°C, and then incubated with secondary antibody 1.5 hat room temperature. Chemo luminescence Substrate was applied to development, and Image J software was used to analyze it.

ChIP-qPCR

ChIP was executed and followed the procedures previously described.[19] Cells were cross-linked with freshly prepared formaldehyde (1.42%) for 10 min, followed by the addition of glycine (125 mM) for 5 min at room temperature. After washing twice with cold phosphate-buffered saline (PBS), cells were scraped and collected by centrifuge. Pelleted cells were resuspended in 400 μL ChIP lysis buffer (50 mM HEPES/KOH, pH 7.5; 140 mM NaCl; 1 mM EDTA; 1% Triton X-100; 0.1% Na-deoxycholate and protease inhibitors) and subjected to sonication with Bioruptor to shear the chromatin (80% power, 20 s on and 40 s off, 18 cycles). After sonication, samples were further diluted with lysis buffer and centrifuged to clear the supernatant. 1/10 of the supernatant was processed to extract total DNA as whole-cell input. The remaining supernatants were incubated with either IgG or YAP antibodies (sc-101199, Santa Cuz) at 4 °C overnight. Samples were added with prewashed protein A/G beads (sc-2003; Santa Cuz) for another 3 h. After that, samples were washed five times with indicated buffers and were mixed with 100 μL of 10% chelex (1421253; Bio-Rad). The samples were boiled for 15 min and centrifuged at 4 °C for 1 min. Supernatants were transferred to new tubes. After that, another 120 μL of MilliQ water was added to each beads pellet, vortex for 10 s, and were centrifuged again to spin down the beads. The supernatants were combined as templates for follow-up qPCR analysis.

ChIP-seq

ChIP-Seq was performed based on a previous protocol with minor modifications.[60] Cells stably expressing Flag-tagged YAP have been subjected to the same treatments as described above to get the cell pellets. After that, cells were resuspended in 400 μL ChIP digestion buffer (20 mM Tris HCl, pH 7.5; 15 mM NaCl; 60 mM KCl; 1 mM CaCl2 and protease inhibitors). Cells were digested with a proper amount of Micrococcal Nuclease (Mnase, M0247S, NEB) to shear chromatin at 37°C for 20 minutes to ensure that the majority of chromatin was mono- and di-nucleosomes. The reaction was stopped with 2X stop buffer (100 mM Tris HCl, pH 8.1; 20 mM EDTA; 200 mM NaCl; 2% Triton X-100; 0.2% Na-deoxycholate and protease inhibitors). Samples were further sonicated with Bioruptor at 80% power for 18 cycles (20 s on and 40 s off). After clarification by centrifugation, soluble chromatin was immunoprecipitated with Flag antibodies (F3165, Sigma) at 4 °C together with prewashed protein A/G beads. After extensive wash with indicated buffers, samples were eluted and reverse cross-linked in elution buffer (10 mM Tris HCl, pH 8.0; 10 mM EDTA; 150 mM NaCl; 5 mM DTT and 1% SDS) at 65 °C overnight. After sequential digestion with Dnase and Proteinase K, DNA was purified using the PCR purification kit (B518141, Sangon Biotech). ChIP'd DNA from three immunoprecipitations were pooled to generate libraries with the Ovation Ultra-Low Library Prep kit (NuGEN) according to the manufacturer's instructions. Sequencing was performed on an Illumina HiSeq 2500 platform.

QUANTIFICATION AND STATISTICAL ANALYSIS

Statistical analysis was performed using SPSS software version 22.0 (SPSS, Chicago, IL). Data are presented as mean ± SD. Differences were analyzed by the Student's t-test and one-way ANOVA. Clinical data were analyzed by Fisher's exact test. Kaplan-Meier method was used to calculate the survival rate and Log-rank test for the different significance. Correlation between the expression of genes was calculated using Pearson correlation. A p-value of<0.05 was considered statistically significant.